Article:
Allen, S., Hall, B., Castelli, L. et al. (2019) Astrocyte adenosine deaminase loss increases motor neuron toxicity in amyotrophic lateral sclerosis. Brain, 142 (3). pp. 586-605. ISSN: 0006-8950

https://doi.org/10.1093/brain/awy353

doi:10.1093/brain/awy353 BRAIN 2019: 142; 586–605 | 586

BRAIN
A JOURNAL OF NEUROLOGY

Astrocyte adenosine deaminase loss increases motor neuron toxicity in amyotrophic lateral sclerosis

Scott P. Allen,[1] Benjamin Hall,[1] Lydia M. Castelli,[1] Laura Francis,[2] Ryan Woof,[1] Alexandros P. Siskos,[3] Eirini Kouloura,[3] Elizabeth Gray,[4] Alexander G. Thompson,[4] Kevin Talbot,[4] Adrian Higginbottom,[1] Monika Myszczynska,[1] Chloe F. Allen,[1] Matthew J. Stopford,[1] Jordan Hemingway,[1] Claudia S. Bauer,[1] Christopher P. Webster,[1] Kurt J. De Vos,[1] Martin R. Turner,[4] Hector C. Keun,[3] Guillaume M. Hautbergue,[1] Laura Ferraiuolo[1] and Pamela J. Shaw[1]

As clinical evidence supports a negative impact of dysfunctional energy metabolism on the disease progression in amyotrophic lateral sclerosis, it is vital to understand how the energy metabolic pathways are altered and whether they can be restored to slow disease progression. Possible approaches include increasing or rerouting catabolism of alternative fuel sources to supplement the glycolytic and mitochondrial pathways such as glycogen, ketone bodies and nucleosides. To analyse the basis of the catabolic defect in amyotrophic lateral sclerosis we used a novel phenotypic metabolic array. We profiled fibroblasts and induced neuronal progenitor-derived human induced astrocytes from *C9orf72* amyotrophic lateral sclerosis patients compared to normal controls, measuring the rates of production of reduced nicotinamide adenine dinucleotides from 91 potential energy substrates. This approach shows for the first time that *C9orf72* human induced astrocytes and fibroblasts have an adenosine to inosine deamination defect caused by reduction of adenosine deaminase, which is also observed in induced astrocytes from sporadic patients. Patient-derived induced astrocyte lines were more susceptible to adenosine-induced toxicity, which could be mimicked by inhibiting adenosine deaminase in control lines. Furthermore, adenosine deaminase inhibition in control induced astrocytes led to increased motor neuron toxicity in co-cultures, similar to the levels observed with patient derived induced astrocytes. Bypassing metabolically the adenosine deaminase defect by inosine supplementation was beneficial bioenergetically *in vitro*, increasing glycolytic energy output and leading to an increase in motor neuron survival in co-cultures with induced astrocytes. Inosine supplementation, in combination with modulation of the level of adenosine deaminase may represent a beneficial therapeutic approach to evaluate in patients with amyotrophic lateral sclerosis.

1 Sheffield Institute for Translational Neuroscience (SITraN), University of Sheffield, 385 Glossop Road, Sheffield S10 2HQ, UK
2 The Living Systems Institute, University of Exeter, Stocker Road, Exeter, EX4 4QD, UK
3 Department of Surgery and Cancer, Imperial College London, Hammersmith Hospital Campus, London W12 ONN UK
4 Nuffield Department of Clinical Neurosciences, Oxford University, John Radcliffe Hospital, West Wing Level 6, Oxford OX3 9DU, UK

Correspondence to: Dr Scott Allen
Sheffield Institute for Translational Neuroscience (SITraN), University of Sheffield, 385 Glossop Road, Sheffield S10 2HQ, UK
E-mail: s.p.allen@sheffield.ac.uk

Received June 18, 2018. Revised October 25, 2018. Accepted November 22, 2018. Advance Access publication January 28, 2019

Keywords: ALS; *C9orf72*; metabolism: inosine: adenosine deaminase

Abbreviations: ALS = amyotrophic lateral sclerosis; HRE = hexanucleotide repeat expansion; iNPC = induced neuronal progenitor cell; NAD(P)H = nicotinamide adenine dinucleotides; RT-PCR = reverse transcriptase polymerase chain reaction

Introduction

Amyotrophic lateral sclerosis (ALS) is an adult-onset disease causing degeneration of upper and lower motor neurons resulting in progressive failure of the neuromuscular system and death typically within 2–3 years of symptom onset. Approximately 10% of all ALS cases and of frontotemporal dementia are associated with a hexanucleotide repeat expansion (HRE) in *C9orf72*. There are three main mechanisms through which the *C9orf72*-HRE has been postulated to contribute to neuronal death: (i) loss of *C9orf72* protein function, which affects autophagy (DeJesus-Hernandez *et al.*, 2011; Webster *et al.*, 2016); (ii) deposition of cytoplasmic dipeptide repeat proteins (DPRs) by sequestration of the nuclear export adaptor SFSR1 onto *C9orf72* repeat transcripts (Mori *et al.*, 2013*a*, *c*; Hautbergue *et al.*, 2017); and (iii) production of expanded RNA species (Mori *et al.*, 2013*b*; Cooper-Knock *et al.*, 2014), with sequestration of RNA-binding proteins (Haeusler *et al.*, 2016).

However, there are several common mechanisms between *C9orf72*-HRE ALS and sporadic ALS including oxidative stress and mitochondrial dysfunction (Lopez-Gonzalez *et al.*, 2016; Onesto *et al.*, 2016; Konrad *et al.*, 2017). ALS is associated with both mitochondrial and metabolic dysfunction, which may influence disease progression as the metabolic pathways are highly susceptible to the disease process, (Haeusler *et al.*, 2016; Tefera and Borges, 2016; De Vos and Hafezparast, 2017; Vandoorne *et al.*, 2018). Increased reactive oxygen species production, lipid peroxidation, mitochondrial uncoupling and membrane depolarization can lead to electron transport chain (ETC) dysfunction, alterations in calcium buffering and reduced ATP generation in both the CNS and in peripheral tissues (Ferraiuolo *et al.*, 2011*b*; Bartolome *et al.*, 2013; Allen *et al.*, 2014, 2015; Raman *et al.*, 2015; Tefera and Borges, 2016; Valbuena *et al.*, 2016; Konrad *et al.*, 2017). Energetically, neurons are supported predominantly by oligodendrocytes and astrocytes (Ferraiuolo *et al.*, 2016; Tefera and Borges, 2016). Astrocytes have a key metabolic role in the CNS: they are the major source of glycogen, and lactate released by astrocytes can be used by motor neurons as a source of energy (Pellerin and Magistretti, 1994). Astrocytes play an important role in ALS disease progression via various mechanisms including reduced lactate release, reduced expression of the glutamate reuptake transporter EAAT2 and release of inflammatory mediators such as nitric oxide and prostaglandin E2 (Lin *et al.*, 1998; Ferraiuolo *et al.*, 2011*a*, *b*). Induced neuronal progenitor cell (iNPC) derived induced astrocytes from sporadic ALS and *C9orf72* patients have been shown to cause toxicity to motor neurons in co-culture (Haidet-Phillips *et al.*, 2011; Meyer *et al.*, 2014; Re *et al.*, 2014). However, the precise manner in which *C9orf72*-HRE affects energy production especially in astrocytes, the mechanisms by which human *C9orf72*-derived astrocytes cause motor neuron toxicity and how these relate to sporadic ALS, are currently unknown.

Many of the dysfunctional metabolic traits associated with ALS correlate with disease duration and survival and are intrinsically linked to the patient's nutritional status (Desport *et al.*, 1999, 2005). As clinical evidence supports a negative impact of dysfunctional energy metabolism on the disease progression in ALS (Desport *et al.*, 2005; Dupuis *et al.*, 2011), it is important to understand how the metabolic pathways could potentially be manipulated to achieve neuroprotective effects. Therefore, the purpose of this study was to test the hypothesis that ALS results in dysfunctional energetic pathways, which can lead to reduced ATP output and an increasing bioenergetic deficit in the CNS. Identification of the specific dysfunctional pathway(s) may allow additional supplementation of the defective energy substrates involved back into the cell to restore the metabolic defect. Alternatively, supplementation of energy substrates downstream of the identified defect would potentially allow the cell to bypass the dysfunction and increase energy production.

Using both patient-derived fibroblasts and iNPC-derived induced astrocytes we have adapted a phenotypic metabolic profiling approach (Bochner *et al.*, 2011) to identify deficient metabolic pathways. This technology enables the comparison of normal versus disease cellular models by simultaneously comparing the rates of energy production from 91 potential energy substrates. This approach has not been used previously in the ALS field and allows a non-biased metabolic screen to be performed on *in vitro* models to identify dysfunctional metabolic pathways by measuring the ability of cells to produce NAD(P)H (nicotinamide adenine dinucleotides). Using this approach, we have identified a novel adenosine metabolism dysfunction caused by reduction of adenosine deaminase (ADA). These data show for the first time, reduced expression of ADA in fibroblasts, in iNPC-derived induced astrocytes and in induced neurons from individuals with *C9orf72* and sporadic ALS. Stimulating the adenosine metabolism pathway downstream with inosine supplementation *in vitro*, increased induced astrocyte bioenergetic flux, increased ATP levels and reduced induced astrocyte-mediated motor neuron toxicity.

Materials and methods

All chemicals were obtained from Sigma unless stated otherwise.

Human biosamples

Experiments were carried out using samples obtained from six *C9orf72*-HRE-positive ALS cases, three sporadic ALS cases and eight matched controls in total (Supplementary Table 1). The average age at time of skin biopsy in ALS cases (five females, four males) was 54 (±12.0) years and 54 (±8.7) years in controls (six females, two males). The average disease duration of the ALS cases was 42.9 (±24.6) months.

Ethical approval

Informed consent was obtained from all human subjects before skin sample collection (Study number STH16573, Research Ethics Committee reference 12/YH/0330). All applicable international, national, and/or institutional guidelines for the care and use of animals were followed.

Human fibroblast cultures

Skin biopsies were obtained from the forearm of subjects after informed consent, in accordance with guidelines set by the local ethics committee. Fibroblast cell cultures were established in supplemented cell culture medium (Lonza) with 10% foetal calf serum (Labtech), 2 mM glutamine, 50 µg/ml uridine, vitamins, amino acids and 1 mM sodium pyruvate in humid incubators at 37°C with 5% CO_2.

C9orf72 cerebral cortical astrocyte mouse culture

Primary cultures of cerebral cortical astrocytes were prepared from *C9orf72*-BAC (C57BL/6) newborn mice (1–2 days old) and were screened for the *C9orf72* expansion using qualitative PCR. Astrocytes were grown to confluence in high glucose (25 mM) Dulbecco's modified Eagle medium (DMEM) containing 10% foetal bovine serum (FBS) and separated from contaminating microglia through shaking and then mild trypsinisation (Saura *et al.*, 2003).

Rodent cortical neuron culture

Cortical neurons were isolated from embryonic Day 18 Sprague Dawley rat embryos (Charles River) and embryonic *C9orf72*-Bac mice (C57BL/6). Neurons were cultured on poly-D-ornithine/poly-L-lysine half-area 96-well plates (Griener) in Neurobasal™ A medium (Thermo Fisher) supplemented with B27 supplement (Invitrogen), 100 IU/ml penicillin (Lonza), 100 mg/ml streptomycin (Lonza), 2 mM L-glutamine, 0.4 mM sodium pyruvate and 25 mM glucose for 10 days prior to metabolic profiling.

Human induced astrocyte and induced neuron culture

Fibroblasts were differentiated as previously described (Meyer *et al.*, 2014). INPCs were cultured in DMEM containing 1% N2 supplement (Life Technologies), 1% B27 and 20 ng/ml fibroblast growth factor-2 (Preprotech). To induce NPC differentiation to induced astrocytes, cells were incubated in a 10 cm dish coated with fibronectin (5 µg/ml, Millipore). Twenty-four hours later the media was changed to DMEM with 10% FBS and 0.3% N2 and allowed to differentiate for 7 days. As published previously (Meyer *et al.*, 2014), this procedure produces induced astrocytes that are 100% positive for vimentin, CD44 and glial fibrillary acidic protein (data not shown). For differentiation into neurons, iNPCs were plated in fibronectin coated (2.5µg/ml) six-well plates and grown to 70–80% confluence after which iNPC medium was removed and replaced with neuron differentiation medium (DMEM/F12 with 1% N2 and 2% B27). On Day 1 post-differentiation, the cells were treated with 2.5 µM DAPT (Tocris) to promote differentiation toward a neuronal lineage. On Days 3–7, the medium was supplemented with 1 µM retinoic acid, 0.5 µM smoothened agonist (SAG) (Millipore) and 2.5 µM forskolin. This method produced 70% β-III tubulin (Tuj1) positive cells (data not shown). Astrocyte/neuronal experiments were repeated at least three times for each line using iNPCs between passages 18 and 25.

Phenotype microarray analysis

Preparation for human fibroblasts

On Day 1, 96-well phenotype microarray plates (PM-M1, Biolog; Supplementary Table 2) had 30 µl of IFM-1 (Biolog) containing 10% dialysed FBS and 0.3 mM glutamine added and then incubated overnight at 37°C/5% CO_2. On Day 2, 96-well half-area plates were coated with 50 µl of fibronectin (0.25 µg/ml in PBS) for 60 min at room temperature and then washed with 100 µl PBS. Confluent fibroblasts were harvested by trypsinisation (Lonza) and the cell number was determined using a trypan blue dye exclusion test and a Countess automated cell counter (Invitrogen). Using the PM-M1 plates incubated the previous day, the IFM-1 fluid now containing the different metabolites was transferred to the corresponding wells on the fibronectin-coated plates. The cells were resuspended at 800 000 cells per ml of IFM-1 media and 20 µl, (equivalent to 16 000 cells), was transferred to each well of the substrate plate and then incubated at 37°C/5% CO_2 for 40 h. After the stated incubation time, 10 µl of redox dye mix MA (Biolog) was added to each well and the plates sealed with sterile Seal-Plate film to stop gas transfer. Dye colour change was measured every 20 min for 120 min and then every 60 min up to 300 min using a BMG Omega Pherastar at 590/790 nM (790 nM was removed from 590 nM to account for background values). After incubation, the plates were washed three times with 100 µl of PBS and stored overnight at −80°C prior to cell counting. All results were normalized to cell number by addition of CyQUANT® (Invitrogen) to each well as per the manufacturer's instructions (1/400 dilution of the dye in HBSS buffer, 100 µl per well) and fluorescence was measured using a BMG Omega FLUOstar.

Preparation for human induced astrocytes

The procedure for induced astrocytes was identical to that for fibroblasts, except for the following: astrocytes at 6 days post-differentiation were harvested by addition of accutase for 3 min. Astrocytes were plated at 10 000 cells per well and incubated for 24 h at 37°C/5% CO_2. After dye addition, the plates were sealed and incubated in an OmniLog™ Phenotype Microarray system at 37°C. The Dye colour change was monitored every 5 min for 355 min for kinetic analysis. All induced astrocytes were analysed from three independent differentiations. For the pentostatin assays, control induced astrocytes were treated with 0.5 µM pentostatin for 24 h in the assay plate prior to adding the redox dye. The assay was then continued as described above.

Preparation for mouse astrocytes

The mouse astrocyte preparation was identical to the fibroblast preparation except that the 96-well plates were coated with 1 µg/ml poly-D-ornithine at 4°C overnight prior to plating the cells and an OmniLog™ Phenotype Microarray system was used to assess dye colour change every 5 min for 355 min.

Preparation of mouse cortical neurons

On Day 9 post-neuronal plating, PM-M1 plates had 50 µl of Neurobasal™ A with B27 and 0.3 mM glutamine added to each well and incubated at 37°C/5% CO_2 overnight. On Day 10, the neuronal media was removed from the cells and replaced with the media from the PM-M1 plate. The cells were then incubated for 40 h prior to addition of 10 µl Redox dye MB (Biolog). The assay was then continued as previously described for the induced astrocytes.

All data had background values removed and subsequently, for fibroblasts, heat maps with hierarchical clustering were generated using Qlucore Omics Explorer 3.0, with time point eliminated as a factor and $P \leqslant 0.05$ taken as significant. Any substrates identified that showed significant toxicity between patients and controls were removed as false positives. Toxicity was assessed by normalizing the specific substrate in question to the positive glucose controls as 100%, using the equation: [(average toxicity assay value) / (average toxicity assay value of glucose)] × 100. The substrates identified using Qlucore underwent further kinetic analysis by two-way ANOVA with Sidak post-test correction at every time point. Initial rate analysis (0–120 min) by linear regression as well as area under the curve analysis was performed on all the kinetic traces on GraphPad Prism (Version 6). All data were analysed from three independent experiments.

Western blot analysis

Cell pellets were washed in PBS and resuspended in 100 µl lysis buffer (89% Radio-Immunoprecipitation Assay buffer, 10% protease inhibitor cocktail and 1% phosphatase inhibitors), on ice. After 30 min, the cells were centrifuged at 13 000 rpm, 4°C for 30 min and the supernatant was collected and retained on ice. Protein content of the supernatant was determined using a Bradford assay as per the manufacturer's instructions. All samples were denatured at 95°C for 5 min in Laemmli buffer and 20 µg of protein was loaded on 10% SDS polyacrylamide gels and protein electrophoresis was performed using Mini-PROTEAN® Tetra Handcast systems (Bio-Rad). Proteins were resolved and transferred to a polyvinylidene difluoride membrane (Millipore) at 250 mM for 60 min before being blocked in 5% bovine serum albumin (BSA) with Tris-buffered saline plus 0.01% Tween (TBST). Primary antibodies used at a dilution of 1/1000 included mouse adenosine deaminase (Santa Cruz D4-sc23846), rabbit LC3 (Novus, NB100-2220), mouse P62 (BD Bioscience, 610833), rabbit NQO1 (Abcam, ab341732) and rabbit actin (Abcam, ab8227). Before detection by chemiluminescence (EZ-ECL HRP kit, Biological Industries) using a G:BOX (Syngene), the membranes underwent 6 × 10 min washes in TBST and were then incubated with secondary anti-rabbit/mouse HRP-linked antibody (1:5000, Cell Signalling Technology) for 60 min. Quantification of protein levels were obtained by densitometry using GeneTools software (version 4.03.05, Syngene). After normalization to the loading controls, patient values were compared to the control value, which was set to 1. For the LC3 blots, LC3-I levels were divided by LC3-II levels to obtain a LC3-I/II ratio.

Quantitative RT-PCR

Extracted RNA samples from three independent differentiations were DNase treated and RNA converted to cDNA as previously described (Hautbergue *et al.*, 2017). The sequences of the *ADA* qPCR primers can be found in the Supplementary material (Note 1). Quantitative RT-PCR reactions were performed in duplicate using the Brilliant III Ultra-Fast SYBR® Green QPCR Master Mix (Agilent Technologies) on a CFX 96™ Real-Time System (Bio-Rad). Quantitative RT-PCR data were analysed using CFX Manager 3.1 (Bio-Rad) and GraphPad Prism using one-way ANOVA with Bonferroni post-test analysis.

Adenosine/inosine cell survival assay

Induced astrocytes were plated in 96-well plates at 10 000 cells per well in 100 µl DMEM containing 5 mM glucose, 0.3 mM glutamine and 10% serum and incubated overnight at 37°C/5% CO_2. The next day 100 µl DMEM with 0.4–13.5 mM adenosine or inosine was added to the plate and incubated for 24 h at 37°C/5% CO_2. Cells were washed three times with 100 µl PBS and stored at −80°C overnight. The next day, the cell number was measured by Cyquant addition as previously described. For the effect of adenosine deaminase inhibition on cell numbers, pentostatin (Cambridge Bioscience) was added to the cells for 18 h at a final concentration of 0.05–50 µM in DMEM. The media was then replaced with DMEM plus 4 mM adenosine and the assay was continued as described above. All assays were performed on three controls and three patient induced astrocyte lines from three different differentiations. All data were compared to the glucose control at 100%, all percentage data were firstly transformed Y = 1/Y, then subsequently Y = logit(Y) prior to Kruskal Wallis analysis with a Dunn's post-test.

ATP assay

Induced astrocytes were plated at 8000 cells per well in 96-well white walled clear-bottomed plates (Greiner) in induced astrocyte media. After 24 h, the media was changed to DMEM media with 5 mM glucose, 10% serum and 0.3 mM glutamine

plus 0.4–13.5 mM inosine. The cells were incubated at 37°C/5% CO_2 for 24 h after which 300 µM iodoacetate (IAA) was added to half of the wells and the cells were then incubated at 37°C/5% CO_2 for 60 min. After 30 min, 1 mM oligomycin was added to half of the wells containing IAA and incubated for 30 min to abolish all ATP production and confirm that the ATP levels in the presence of IAA were produced by the mitochondrial ATP synthase. Subsequently, the media was removed from the wells and cellular ATP was measured using an ATPlite assay kit (PerkinElmer) as per the manufacturer's instructions. The plate was read on a BMG Pherastar plate reader on luminescence mode. Cell numbers were normalized by adding Cyquant to all the wells and incubating for 60 min at 37°C/5% CO_2. Cell counts were read on a BMG Pherastar plate reader at 485 nm excitation 520 nm emission. Fibroblast ATP assays were performed in the same way except that inosine was incubated for 40 h prior to IAA being added. Total ATP levels were determined as well as the oxidative phosphorylation specific ATP levels (ATP levels in the presence of IAA which are oxidative phosphorylation specific as they are abolished in the presence of IAA and oligomycin; data not shown). Glycolytic ATP was determined by subtracting oxidative phosphorylation-specific ATP from total ATP. All assays were performed on three controls and three patient induced astrocyte lines from three different differentiations and analysed by one way ANOVA with a Bonferroni post-test analysis.

Seahorse XF24 bioanalyser assay

Induced astrocytes were plated at 15 000 cells per well in a 24-well Seahorse cell culture plate (Agilent/Seahorse Bioscience) in induced astrocyte cell culture media and incubated overnight at 37°C/5% CO_2. The next day the media was replaced with DMEM media with 5 mM glucose, 10% serum, 0.3 mM glutamine and inosine at 1.0–13.5 mM. The cells were incubated at 37°C/5% CO_2 for 24 h. The next day the media was replaced with Seahorse media pH 7.4 (Agilent/Seahorse Bioscience) containing inosine and incubated at 37°C in a non-CO_2 incubator for 60 min. The effect on oxygen consumption rate and extracellular acidification rate was measured four times for 2.5 min each in the absence and presence of oligomycin (to determine coupled respiration and glycolytic capacity), FCCP, and finally antimycin A in combination with rotenone. To allow normalization, cell numbers were determined by the addition of Cyquant to the cells as previously described. All data were analysed by Kruskal Wallis analysis with a Dunn's post-test.

Lactate assay

Lactate levels were measured using a Promega Lacate-Glo™ assay kit on fibronectin coated 384-well plates. induced astrocytes were plated at 10 000 cells per well in 30 µl of DMEM containing 5 mM glucose, 0.3 mM glutamine and 10% dialysed serum and then incubated at 37°C/5% CO_2. 24 h later, DMEM ± 4 mM inosine was added and the plate was incubated for a further 24 h at 37°C/5% CO_2. The media was then removed and the assay was continued as per the manufacturer's instructions. Lactate levels were measured on a BMG PHERAstar plate reader with cell numbers measured by adding Cyquant as described previously. All assays were performed on three controls and three patient induced astrocyte lines from three different differentiations and analysed by one-way ANOVA with a Bonferroni post-test analysis.

Uric acid assay

C9orf72 induced astrocytes and controls were differentiated as described previously in six-well dishes. On Day 6 post differentiation, the media was changed to DMEM with 5 mM glucose, 10% serum and 0.3 mM glutamine, ±4 mM inosine. The plates were incubated for 24 h at 37°C/5% CO_2, prior to being harvested and stored at −80°C. On the day of the assay, samples were homogenized in 125 µl of cold uric acid assay buffer for 20 min on ice and then centrifuged at 13 000*g* for 10 min at 4°C to remove insoluble material. Protein content was assessed using a Bradford assay as per the manufacturer's instructions. Uric acid standards for colorimetric detection at 0 (blank), 2, 4, 8, 16, 24, 32, and 40 nmol/well in 50 µl uric acid buffer were added to the plate in duplicate as well as the patient samples. Fifty microlitres of a master mix containing 46 µl assay buffer, 2 µl uric acid probe and 2 µl enzyme mix were added to each well. The plate was incubated in the dark for 30 min at 37°C, prior to detection on a BMG PHERAstar at 570 nm.

Induced astrocyte EGFP motor neuron viability co-culture assay

On Day 1, 1500–3000 induced astrocytes were seeded in 25 µl DMEM containing 5 mM glucose, 10% serum and 0.3 mM glutamine on fibronectin-coated black 384-well plates and incubated at 37°C/5% CO_2 for 24 h. On Day 2, 0.1–13.5 mM inosine was added and then incubated as described for a further 24 h. On Day 3, 2500 murine Hb9-EGFP + motor neurons (a kind gift from Tom Jessell, Columbia University, New York) per well were seeded on top of the pretreated induced astrocytes. Hb9-GFP + motor neurons were imaged after 24, 48 and 72 h using an IN Cell Analyzer 2000 (GE Healthcare), and the number of viable motor neurons were counted using the Columbus analyser software. The number of viable motor neurons (defined as GFP + motor neurons with at least one axon) that survive after 72 h in co-culture was calculated as a percentage of the number of viable motor neurons after 24 h in co-culture. One-way ANOVA with Bonferroni *post hoc* test was then performed. For the pentostatin assays, induced astrocytes were treated with 0.05/0.5/5 µM pentostatin for 18 h prior to the addition of adenosine to the cells. Pentostatin media was removed from the cells and replaced with media containing 4 mM adenosine for 24 h prior to adding the motor neurons. Cell survival was assessed as described up to 48 h. All assays were performed on three controls and three patient induced astrocyte lines from at least four different differentiations.

Data availability

Raw data were generated at The University of Sheffield. Derived data supporting the findings of this study are available from the corresponding author on request.

Results

C9orf72-HRE leads to reduced NADH production with adenosine in fibroblasts and induced astrocytes

We used a novel screening approach to identify substrates that had significantly different NADH production in the *C9orf72* ALS models compared to controls. To identify the substrates in question for further kinetic analysis, data from the screens were analysed using Qlucore to generate heat maps (Supplementary Fig. 1) and all identified substrates were analysed by two-way ANOVA, area under the curve (AUC) analysis and initial rate analysis to identify significant hits. Using this stringent analytical approach, five energy substrates—fructose, adenosine, pyruvic acid, galactose and succinamic aci—were identified as being hypometabolic in the *C9orf72* cases compared to controls (Fig. 1A, B and Supplementary Fig. 2A–C). Two fructose disaccharides lactulose and palatinose were identified as hypermetabolic in the *C9orf72* cases compared to controls (Supplementary Fig. 2D and E). All the substrates showed an overall significant difference between controls and *C9orf72* cases (using two-way ANOVA) and a significant difference at one-time point or more (Sidak post-test analysis). Both control and *C9orf72* fibroblasts were reprogrammed into iNPCs before differentiation into induced astrocytes. *C9orf72* has been shown to play a key role in the initiation of autophagy, with decreased autophagy observed in *C9orf72* models of disease including induced neurons and accumulation of the p62 protein observed in CNS cell models and CNS tissue from ALS patients (Al-Sarraj *et al.*, 2011; Webster *et al.*, 2016). The *C9orf72* induced astrocytes used in this study displayed *C9orf72* specific cellular dysfunction such as raised p62 levels (Supplementary Fig. 3A and B), an elevated LC3-I/II ratio indicating disruption in the autophagy pathway (Supplementary Fig. 3C and D) and reduced levels of NQO1 [NAD(P)H dehydrogenase quione1], indicating potentially a reduced antioxidant response (Supplementary Fig. 3E and F). When we phenotypically screened the iNPC-derived induced astrocytes, unlike the fibroblasts, the *C9orf72* induced astrocytes were susceptible to starvation-induced toxicity (data not shown) and were only able to metabolise on average nine of the energy substrates in addition to the glucose control. Therefore, Qlucore analysis was not appropriate due to the high number of false positives produced. We focused our analysis on the substrates that were successfully used by at least two out of the three *C9orf72* induced astrocytes patient lines. Of those nine substrates, five were hypometabolic to varying degrees in the *C9orf72* patient-derived induced astrocytes compared to controls (Fig. 1, Supplementary Figs 4A–F and 5A–F). As with the fibroblasts, fructose, adenosine and pyruvic acid were identified as significantly hypometabolic (by two-way ANOVA) in two of three *C9orf72* cases compared to controls [the remaining Patient (Patient 183) showed significant levels of toxicity in the presence of all these metabolites and the data were not included in the analysis]. In addition, glycogen and dextrin showed reduced NADH production in the induced astrocytes; however, this did not reach significance when performing two-way ANOVA (Supplementary Fig. 4B and C). The remaining substrates showed no significant difference in NADH production between controls and patients (Supplementary Fig. 4 D-F), including inosine (Fig. 1F), which mimicked what was observed in *C9orf72* fibroblasts (Fig. 1C). As adenosine undergoes deamination by adenosine deaminase (ADA) to produce inosine and the known pathways for NADH-based energy production from both inosine and adenosine is via metabolism to ribose-phosphate and eventually glycolysis, this pathway warranted further investigation.

Reduced levels of adenosine deaminase are observed in ALS patient cells

To assess whether levels of ADA were altered in the *C9orf72*-HRE cellular models, which might contribute to adenosine hypometabolism, we used western blot analysis to measure ADA levels in fibroblasts, induced astrocytes and induced neurons. Overall, ADA levels were significantly lower in *C9orf72* fibroblasts (Supplementary Fig. 2F and G), induced astrocytes (Fig. 2A and B) and induced neurons (Fig. 2C and D). Patient 201 had the highest protein level of ADA across all three cell models in the *C9orf72* patients including the iNPCs (Supplementary Fig. 3G and H), whilst Patient 183 had the lowest. This consistency was also observed at the mRNA level, with Patient 183 showing the lowest mRNA levels in induced astrocytes and induced neurons. Overall the level of *ADA* mRNA was significantly reduced in induced astrocytes but not induced neurons ($P = 0.080$; Fig. 2I and J), which reflected the western blot data. As HRE-driven *C9orf72* ALS accounts for a significant portion of both familial and apparently sporadic ALS cases, common mechanisms of dysfunction are likely to exist between the two currently described distinct subgroups of ALS. To answer the question of whether the adenosine metabolism pathway was one possible common mechanism, we measured ADA levels in three sporadic ALS patient-derived induced astrocyte cell lines. As with the *C9orf72* induced astrocytes, a significant reduction in ADA was observed in the sporadic ALS cases at the protein level primarily driven by Patients sALS-9 and sALS-12 (Fig. 2E and F). A reduction of *ADA* was also observed at the mRNA level but this did not reach significance ($P = 0.086$; Fig. 2I). We repeated these experiments in sporadic ALS induced neurons and found comparable results both at the protein and mRNA level (Fig. 2G, H and J). To assess whether reduced NADH production was also evident in sporadic ALS induced astrocytes in the presence of adenosine, we screened the patient cohort as previously

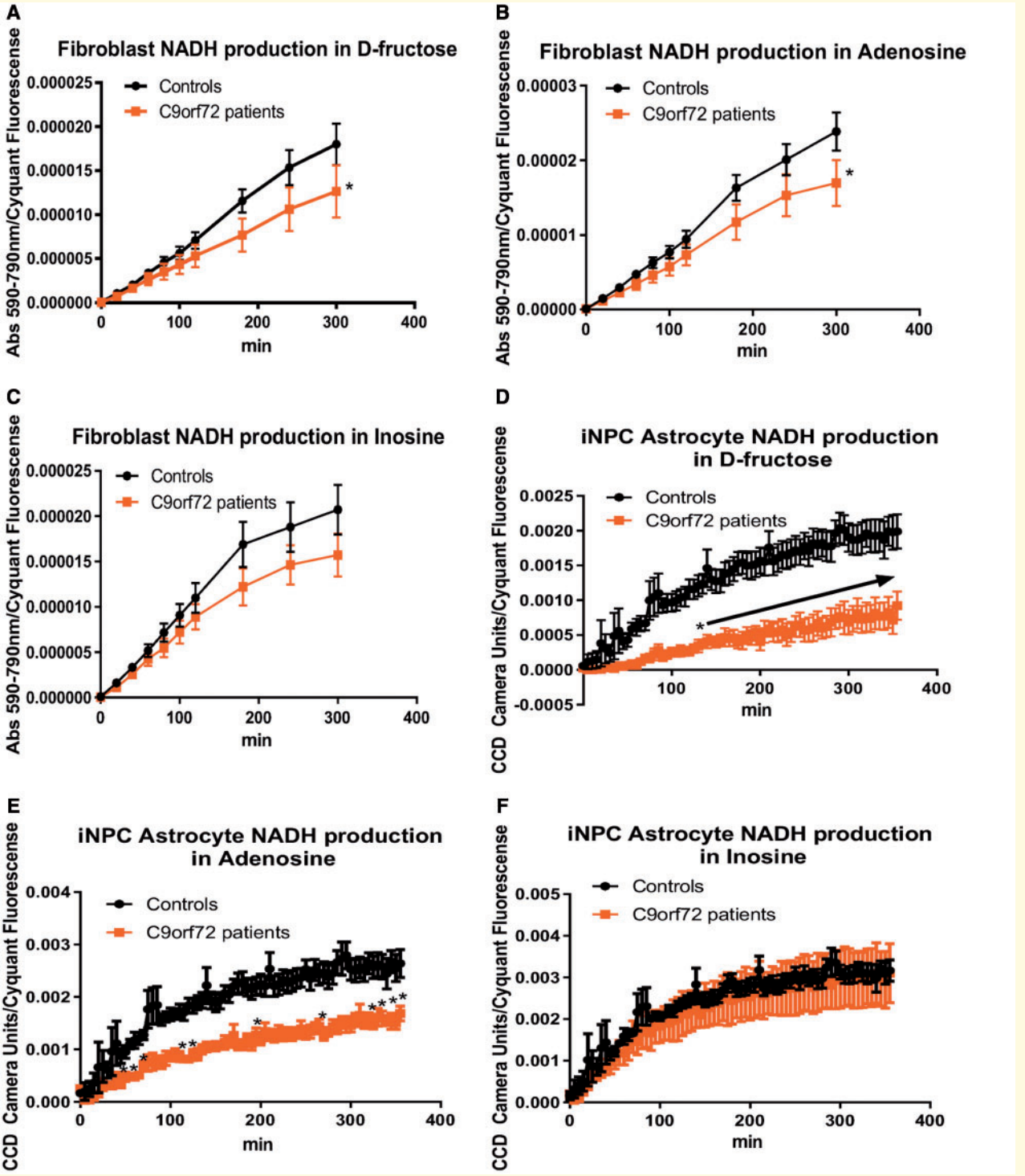

Figure 1 NADH production kinetic analysis of the top hits from the fibroblast and astrocyte phenotypic metabolic screen. (**A**) NADH production in fibroblasts with D-fructose as the sole energy source. (**B**) NADH production in fibroblasts with adenosine as the sole energy source. (**C**) NADH production in fibroblasts with inosine as the sole energy source. (**D**) NADH production in induced astrocytes (iAstrocytes) with D-fructose as the sole energy source. (**E**) NADH production in induced astrocytes with adenosine as the sole energy source. (**F**) NADH production in induced astrocytes with inosine as the sole energy source. Controls depicted in black and *C9orf72* patients in orange. Fibroblast NADH production was measured using a BMG PHERAstar plate reader taking absorbance readings every 15 min over a 6-h period. Induced astrocyte NADH production was measured using an OmniLog™ metabolic profiling system, taking readings every 5 min over a 6-h period. Data presented as mean with standard error, for eight controls and six patients in triplicate for the fibroblasts and three controls and three patients for the induced astrocytes in triplicate. Background intensity values were subtracted from raw data values before being normalized to cell number (by Cyquant analysis). To detect differences in NADH production between controls and patients, two-way ANOVA, with Sidak post-test, area under the curve (AUC) and initial rate analysis by linear regression was performed. *$P \leqslant 0.05$, multiple consecutive significant time points are represented as arrows. For all AUC and rate analyses see Supplementary Table 3.

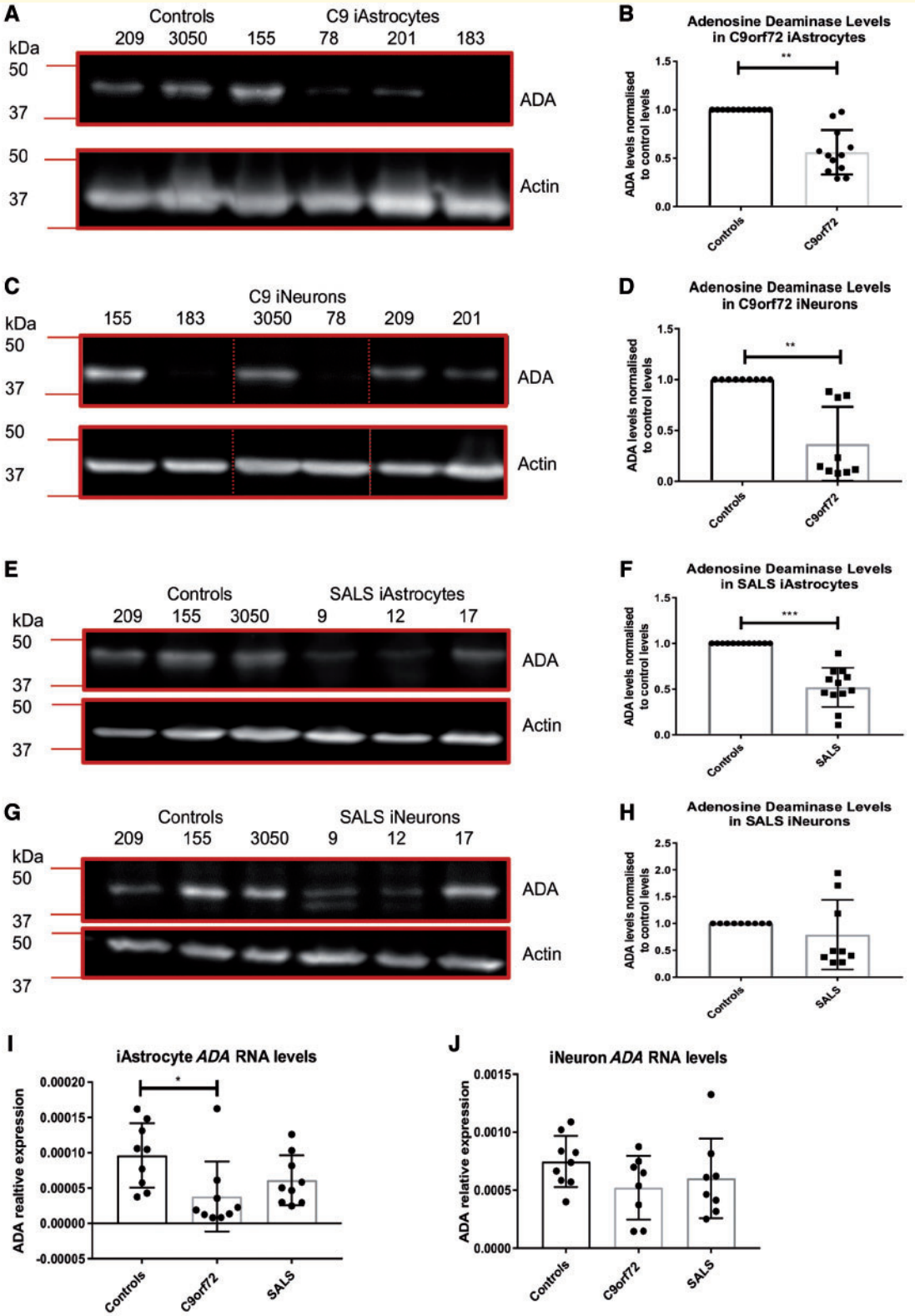

Figure 2 RNA and protein levels of adenosine deaminase (ADA) are reduced in *C9orf72* and sporadic ALS patient cell models. (**A** and **E**) Western blot in human induced astrocytes. (**B** and **F**) induced astrocyte densitometry analysis. (**C** and **G**) Western blot in human induced neurons. (**D** and **H**) Induced neuron (iNeuron) densitometry analysis. (**I**) RT-PCR analysis of *ADA* RNA levels in induced astrocytes. (**J**) RT-PCR analysis of *ADA* RNA levels in induced neurons. Densitometry analysis performed by normalizing the *ADA* levels to the actin loading control and setting the control values to one then comparing the patient value to the matched control value. Representative western blots of three controls versus three patients performed $n = 3/4$ before densitometry analysis by Wilcoxon matched rank analysis. $^{*}P \leqslant 0.05$, $^{**}P \leqslant 0.01$, $^{***}P \leqslant 0.001$. Individual RT-PCR data presented with mean and standard deviation followed by unpaired *t*-tests. Dashed lines = indicates cropped image. For full length gels see the Supplementary material.

described (Supplementary Figs 5G–I and 6A–G). As with the *C9orf72* induced astrocytes, the sporadic ALS induced astrocytes were able to use fructose, inosine, dextrin, glycogen and pyruvic acid to varying degrees (as well as glucose, maltotriose, mannose and maltose, data not shown). As with the *C9orf72* induced astrocytes, the sporadic ALS induced astrocytes showed no inosine metabolism defect but a strong adenosine metabolism defect in two of three patients, leading to cell death (Supplementary Fig. 6A and C). Cell line sALS-17, which had the highest ADA levels out of all the ALS patients, also showed the highest NADH production in adenosine, which was statistically indistinguishable from the controls.

Adenosine causes toxicity in ALS astrocytes which can be replicated in controls by ADA inhibition

Adenosine has been shown to be toxic to embryonic stem cell-derived motor neurons in the presence and absence of wild-type astrocytes (Ng *et al.*, 2015). With this is mind we supplemented the iNPC-derived induced astrocyte cultures with increasing levels of adenosine and inosine and measured cell numbers 24 h later (Fig. 3). *C9orf72* and sporadic ALS induced astrocytes were more susceptible to adenosine induced cell loss than control induced astrocytes (Fig. 3A), with ~60–80% cell loss when exposed to >4 mM adenosine, compared to 40% in the controls. In contrast, inosine supplementation produced very little cell loss in any lines, comparable with just adding more glucose to the cells (data not shown) indicating that the cell loss at the top concentration of 13.5 mM was likely to be due to mild osmotic shock. To assess whether the level of ADA at the protein level was protective, we correlated the level of ADA expression in the patient induced astrocytes with cell survival observed in the adenosine toxicity assays (Fig. 3C). The level of cell survival positively correlated with relative ADA expression ($R^2 = 0.889$, $P = 0.0048$), whereas no significant correlation was observed in control-derived cell lines (data not shown). Inhibition of ADA in induced astrocytes with the irreversible inhibitor pentostatin in the absence of adenosine did not affect cell numbers (data not shown). In the presence of adenosine, however, the control lines showed increased sensitivity to pentostatin-induced cell loss (Fig. 3D), with cell numbers (above 5 μM pentostatin) reduced to similar levels observed in *C9orf72* induced astrocytes in the presence of adenosine. As expected, *C9orf72* induced astrocytes showed increased sensitivity to pentostatin with 0.05 μM of the inhibitor sufficient to cause a 60% drop in cell number (Fig. 3E). To assess whether lower ADA activity resulted in reduced adenosine metabolism, we measured NADH production in control induced astrocytes treated with pentostatin for 24 h prior to running the screening assay. We found that NADH production in the presence of adenosine was significantly reduced in control induced astrocytes treated with pentostatin compared to the dimethyl sulphoxide (DMSO) control (Fig. 3F), whilst inosine metabolism was unaffected (Supplementary Fig. 4G). These results indicate that reduced levels of ADA lead to reduced adenosine metabolism causing a decrease in bioenergetic output and induced astrocyte cell death in the presence of elevated levels of adenosine. With this is mind we next investigated the possibility that supplementing ALS induced astrocytes with inosine may bypass the adenosine metabolism defect and be beneficial bioenergetically.

Supplementation of induced astrocytes with inosine leads to increased bioenergetic capacity

Inosine supplementation of induced astrocyte cultures increased total ATP levels in both control and patient fibroblasts and induced astrocytes (Fig. 4A and Supplementary Fig. 2H). In control induced astrocytes, inosine increased ATP predominantly via the mitochondria and to a lesser extent through glycolysis (11% increase), whilst in patient induced astrocytes the opposite was true (Fig. 4B and C). This difference in metabolic response to inosine supplementation may be due to a metabolic shift in *C9orf72* induced astrocytes as observed previously in fibroblasts from SOD1 patients (Allen *et al.*, 2014). To test this, we calculated the metabolic equilibrium (which we define as the amount of ATP produced by glycolysis compared to the mitochondria as a percentage of the total) in control and *C9orf72* induced astrocytes (Fig. 4D and E). In control induced astrocytes under standard glucose conditions, 33% of the total ATP was produced via the mitochondria indicating as expected a predominantly glycolytic metabolic state. However, in the presence of 4 mM inosine and above, mitochondrial ATP accounted for ~50% of the total ATP output indicating that inosine supplementation shifted the metabolic equilibrium to a more aerobic state in control induced astrocytes, which was not observed by supplementing with additional glucose (Fig. 4D). In contrast, under glucose conditions, the *C9orf72* induced astrocytes were more glycolytic in nature, with on average only 17% ATP produced aerobically, almost half that observed in controls (Fig. 4D and E). Moreover, inosine supplementation had no effect on the metabolic equilibrium of *C9orf72* induced astrocytes in contrast to control induced astrocytes. To confirm this, we used a XF24 metabolic bioanalyser to assess the effect of inosine supplementation on mitochondrial respiratory rates and glycolytic flux rates in induced astrocytes. In control induced astrocytes, inosine supplementation increased the coupled respiratory flux rate by 27% without reaching significance (Fig. 4F). However, inosine supplementation increased not only glycolytic flux rates but also glycolytic capacity flux rates in control induced astrocytes (Fig. 4G and H), suggesting that although glycolytic rates increased by 80% with inosine supplementation in controls, this only led to a 11% increase in

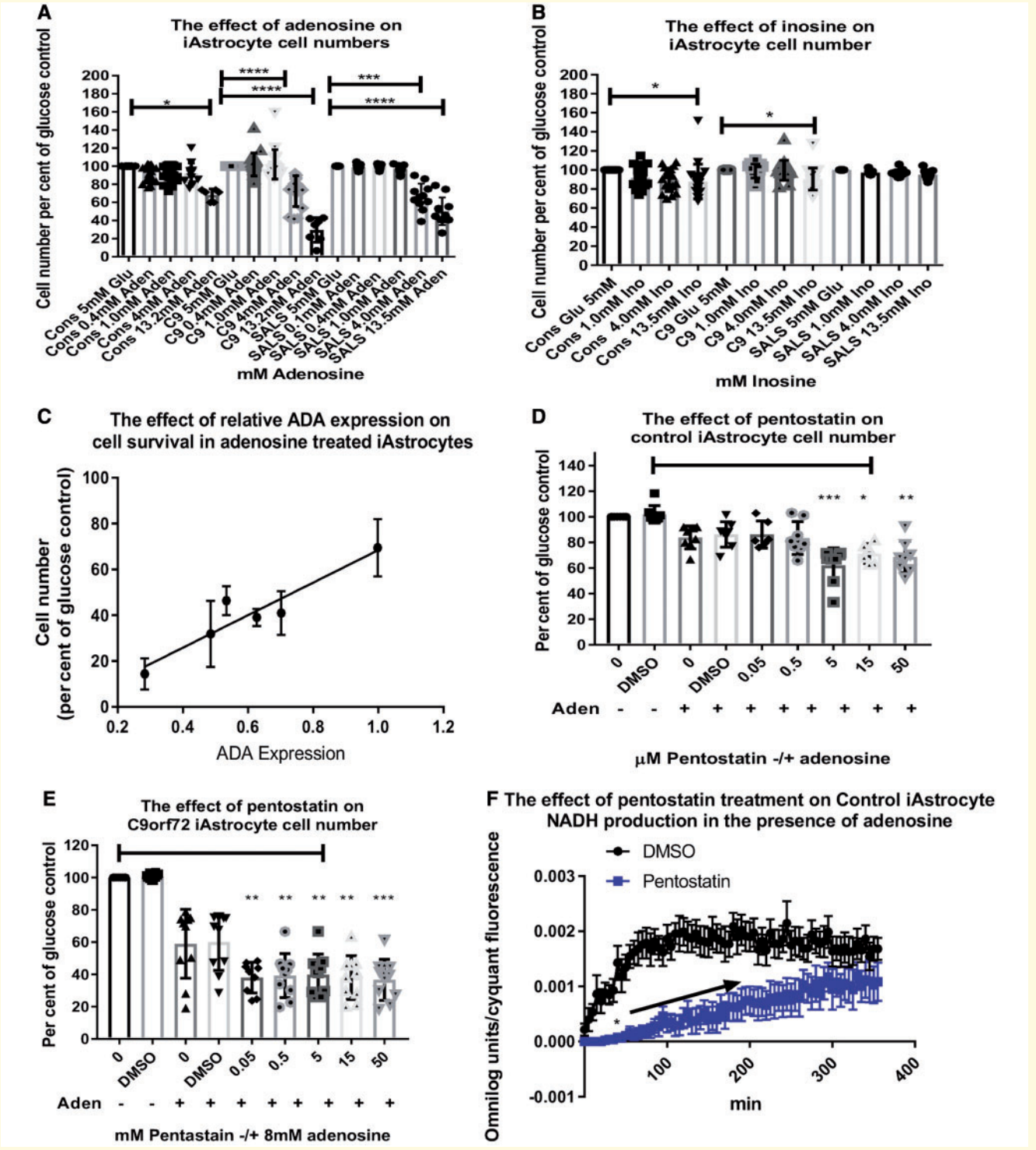

Figure 3 ***C9orf72* and sporadic ALS induced astrocytes are more susceptible to adenosine-mediated toxicity.** (**A**) The effect of adenosine supplementation on induced astrocyte cell number. (**B**) The effect of inosine supplementation on induced astrocyte cell number. (**C**) The effect of ADA expression on adenosine mediated toxicity, analysed by Pearson's correlation analysis ($R^2 = 0.8891$, $P = 0.0048$, 95% confidence intervals = 0.5597 to 0.9939). (**D**) The effect of 4 mM adenosine on control induced astrocytes after pentostatin treatment. (**E**) The effect of 4 mM adenosine on *C9orf72* induced astrocytes after pentostatin treatment. All data normalized to glucose control at 100%, each data point indicates one cell line performed once, all assays performed on three controls and three patient astrocyte lines in triplicate. Data transformed Y = 1/Y and Y = Logit(Y) prior to Kruskal Wallis analysis with a Dunn's post-test. *$P \leqslant 0.05$, **$P \leqslant 0.01$, ***$P \leqslant 0.001$, ****$P \leqslant 0.0001$. Cons = controls; C9 = *C9orf72* patients; Glu = glucose. (**F**) The effect of pentostatin treatment on control induced astrocyte NADH production in the presence of adenosine. For AUC and rate analysis see Supplementary Table 3. Data presented as mean with standard error, controls $n = 3$ in triplicate. Background intensity values were subtracted from raw data values before being normalized to cell number (by Cyquant analysis). Two-way ANOVA, with Sidak post-test, area under the curve (AUC) and initial rate analysis by linear regression was performed to detect differences in NADH production between DMSO and pentostatin treated cells. *$P \leqslant 0.05$.

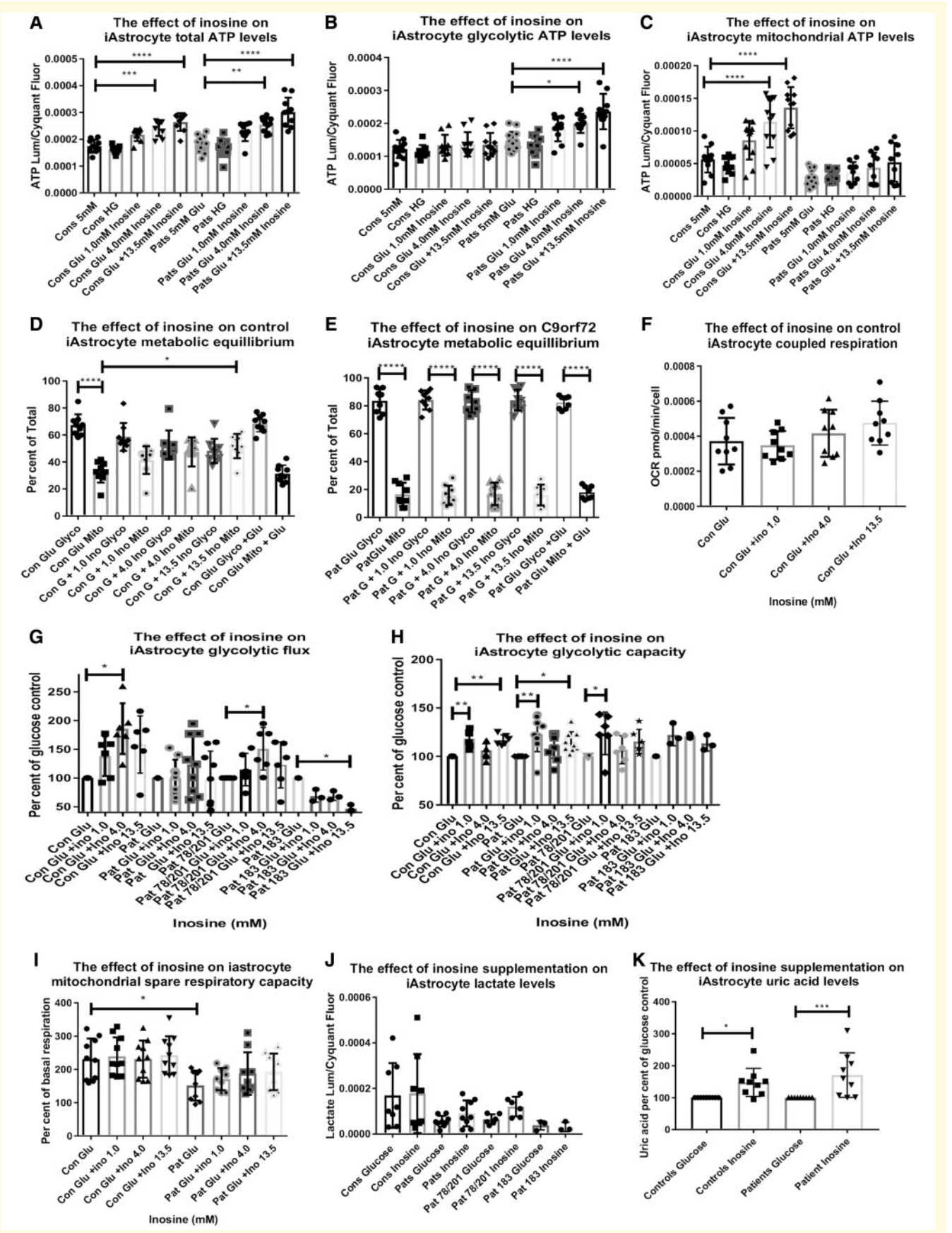

Figure 4 Inosine supplementation increase glycolytic energy output in *C9orf72* induced astrocytes. (**A**) The effect of inosine supplementation on total ATP levels. (**B**) The effect of inosine supplementation on glycolytic ATP levels. (**C**) The effect of inosine supplementation

(continued)

glycolytic ATP levels; the reasons for this are presently unclear. In patient induced astrocytes, inosine supplementation did not affect coupled respiratory flux rates (data not shown). However, the spare respiratory capacity flux reduction we observed between patients and controls was lost upon inosine supplementation (Fig. 4I) confirming the mild increase in mitochondrial ATP data (Fig. 4C). Inosine supplementation significantly increased glycolytic capacity and showed a trend for an increase in glycolytic flux rates (Fig. 4G and H). Interestingly, we noticed a differential glycolytic flux response in Patient 183 after inosine supplementation compared to Patients 78 and 201, which when grouped together showed a significant increase in glycolytic flux and glycolytic capacity rates (Fig. 4G and H). This muted response in Patient 183 was also observed when we analysed lactate production in the patient induced astrocytes after inosine supplementation (Fig. 4J). Inosine treatment increased lactate production in *C9orf72* induced astrocytes by ~60%; however, this did not reach significance as inosine treatment did not increase lactate levels in Patient 183, whereas an increase in lactate production was observed in Patients 78 and 201, which reached significance when performing an unpaired *t*-test ($P = 0.0185$). We also measured extracellular lactate levels after inosine supplementation, which showed similar (patient-specific) results to the intracellular lactate levels but no overall significance (data not shown). To assess whether inosine supplementation was also bioenergetically beneficial in the sporadic ALS induced astrocytes as well as *C9orf72* induced astrocytes, we supplemented the induced astrocytes with inosine and measured ATP output. As observed in the *C9orf72* induced astrocytes, inosine supplementation generally increased total ATP levels in a patient-specific manner in the sporadic ALS induced astrocytes, which reached significance in Patient sALS-12 (Supplementary Fig. 6H). Patients sALS-12 and sALS-17 showed an increase or a trend towards an increase in both mitochondrial and glycolytic ATP output in the presence of inosine (Supplementary Fig. 6I and J), while Patient sALS-9 showed no increase in glycolytic ATP (Supplementary Fig. 6J). The increase in cellular ATP levels in response to inosine supplementation was AMP-activated protein kinase (AMPK) independent as supplementation did not affect the level of phosphorylated AMPK protein in either fibroblasts or induced astrocytes (as assessed by western blot, data not shown). Moreover, inosine supplementation did not affect the levels of phosphofructokinase-1, (the rate-limiting enzyme in glycolysis), pyruvate dehydrogenase (PDH) and PDH kinase levels (PDK4) in induced astrocytes.

An alternative pathway for inosine metabolism is conversion to uric acid via xanthine (Fang *et al.*, 2013). To assess whether inosine supplementation in induced astrocytes activated this pathway, we measured uric acid levels in control and *C9orf72* induced astrocytes treated with 4 mM inosine for 24 h (Fig. 4K). Inosine supplementation significantly increased uric acid levels in both control and patient-derived induced astrocytes.

Pretreatment of induced astrocytes with inosine leads to increased motor neuron survival in co-culture

To assess whether the positive effect of inosine supplementation on the bioenergetic profile of induced astrocytes was beneficial to neurons, induced astrocytes were treated with inosine at varying concentrations in the presence of glucose for 24 h prior to the addition of EGFP-labelled mouse motor neurons. Survival of the neurons was assessed over a 72-h period using a fluorescent readout on an IN Cell Analyzer. In the presence of control induced astrocytes, 40–50% of the motor neurons were alive after 72 h, with the loss of motor neurons most likely caused by cellular mechanisms induced by the co-culturing of mouse neurons with human astrocytes or perhaps species incompatibility at induced astrocyte motor neuron contact sites. Typically, and as reported previously (Meyer *et al.*, 2014), *C9orf72* induced astrocytes were less supportive to motor neurons than control induced astrocytes, leading to 30–40% increase in neuronal death after 72 h, compared to controls (Fig. 5A). Inosine supplementation in both control and patient induced astrocytes led to a significant increase in motor neuron survival in a dose-dependent manner (Fig. 5A). However, as with both the lactate and glycolytic flux assays, the level of motor neuron survival in inosine was patient-specific (Fig. 5B–G). Patient 78 and 201 after inosine supplementation each showed a unique dose profile, shown independently in Fig. 5, while inosine treatment in Patient 183 did not alter the level of toxicity towards motor neurons. Inosine supplementation in the sporadic ALS induced astrocytes led to a significant increase in motor

Figure 4 Continued
on mitochondrial ATP levels. (**D**) The effect of inosine supplementation on control induced astrocyte metabolic equilibrium. (**E**) The effect of inosine supplementation on *C9orf72* induced astrocyte metabolic equilibrium. (**F**) The effect of inosine supplementation on mitochondrial coupled respiration. (**G**) The effect of inosine supplementation on glycolytic flux. (**H**) The effect of inosine supplementation on glycolytic capacity flux. (**I**) The effect of inosine supplementation on spare respiratory capacity flux. (**J**) The effect of inosine supplementation on cellular lactate levels. (**K**) The effect of inosine supplementation on cellular uric acid levels. Induced astrocytes (iAstrocytes) were supplemented with inosine for 24 h. Each data point indicates one cell line performed once. All assays were performed on three controls and three patient astrocyte lines in triplicate. All data were analysed by Kruskal Wallis analysis with a Dunn's post-test. $^{*}P \leqslant 0.05$, $^{**}P \leqslant 0.01$, $^{***}P \leqslant 0.001$, $^{****}P \leqslant 0.0001$. Cons = controls; Pats = *C9orf72* patients; Glu = glucose; HG = high glucose (16 mM).

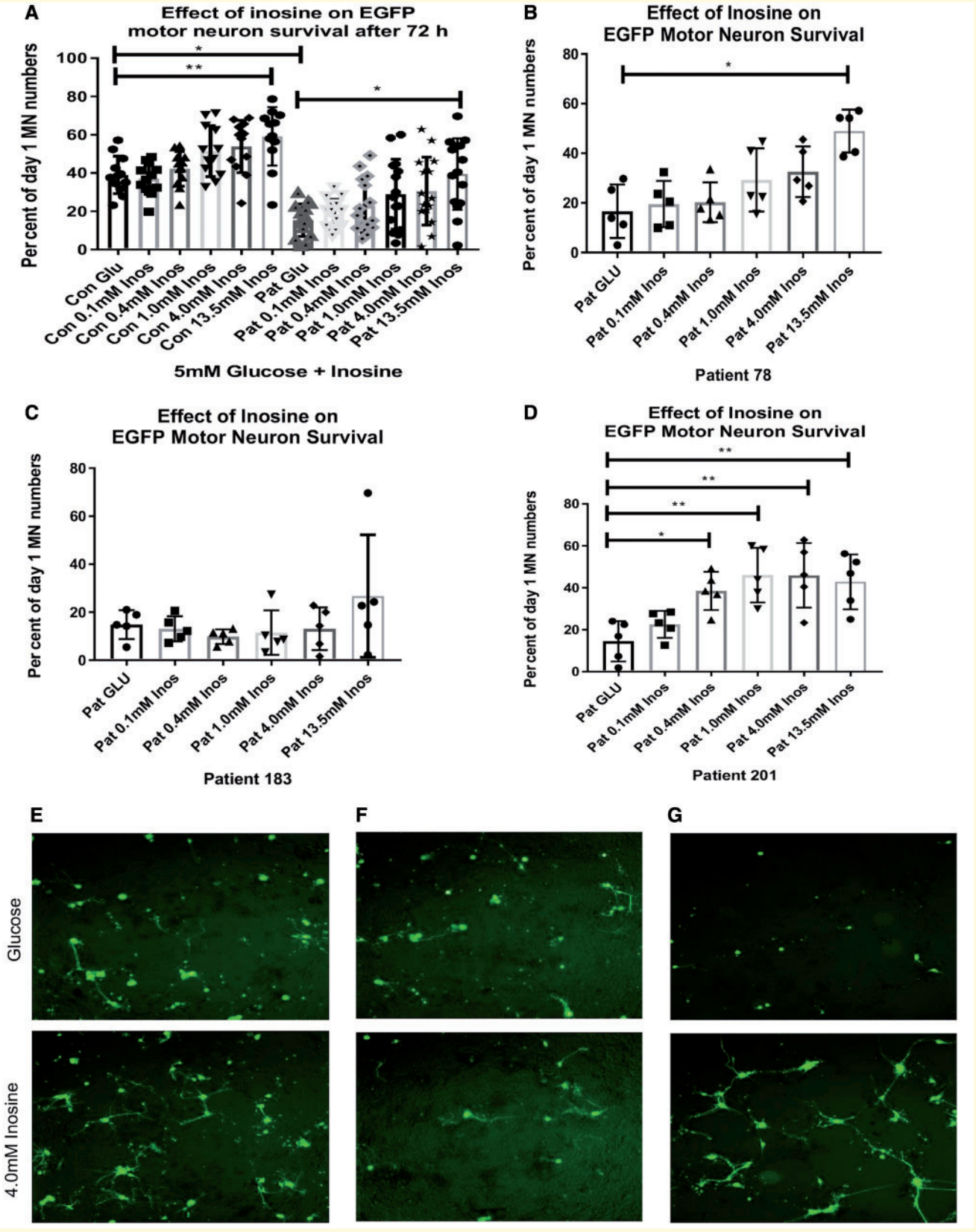

Figure 5 ***C9orf72*** **induced astrocyte inosine supplementation increases motor neuron survival in co-culture.** Induced astrocytes (iAstrocytes) were treated with 0.4–13.5 mM inosine for 24 h prior to 72 h co-culture with EGFP motor neurons (MN). (**A**) Number of motor neurons with axons after 72 h expressed as a percentage of the number alive at the start of the assay. (**B**–**D**) Number of motor neurons with axons after 72 h expressed as a percentage of the number alive at the start of the assay for Patients 78, 183 and 201. (**E**–**G**) Representative images of the motor neurons after 72 h in glucose (5 mM) or glucose + inosine (4 mM). All data were transformed Y = 1/Y and Y = Logit(Y) prior to Kruskal Wallis analysis with a Dunn's post-test and are presented with mean and standard deviation. $*P \leqslant 0.05$, $**P \leqslant 0.01$.

neuron survival in Patients sALS-12 and sALS-17, again in a patient-specific manner (Fig. 6). In common with Patient 183, inosine supplementation in Patient sALS-9 did not lead to a significant increase in motor neuron survival (Fig. 6A and B). However, as with Patient 183, inosine did not increase glycolytic energy production in Patient sALS-9 indicating a common non-response mechanism. To assess whether ADA levels affected the induced astrocyte toxicity towards motor neurons, we correlated ADA expression levels in *C9orf72* and sporadic ALS induced astrocytes with motor neuron survival in co-culture (Fig. 6G). Under glucose conditions, we found no positive correlation. In the presence of inosine, however, we found a positive correlation between induced astrocyte ADA levels and motor neuron survival, which reached significance at 0.4 and 1.0 mM inosine, ($R^2 = 0.895$, $P = 0.0160$, $R^2 = 0.860$, $P = 0.0280$, respectively). When assessing the effect of inosine supplementation on motor neurons alone, supplementation had no effect on survival (Supplementary Fig. 7A and B). Therefore, the inosine supplementation-induced decrease in motor neuron toxicity appeared to be primarily driven by astrocyte metabolism. This was confirmed by assessing NADH production in the presence of inosine in mouse cortical neurons compared to mouse cortical astrocytes (Supplementary Fig. 7C and D). Mouse cortical neurons showed minimal NADH production in the presence of inosine compared to glucose, while mouse cortical astrocytes showed much higher NADH production with inosine. Rat cortical neurons also showed minimal NADH production in the presence of inosine compared to glucose (Supplementary Fig. 7E).

Our co-culture results suggest that efficient metabolism of endogenous adenosine to inosine is important for induced astrocyte support of motor neurons and that stimulating this pathway by supplementing with inosine may reduce induced astrocyte-mediated toxicity. To assess whether functional ADA plays a role in this toxic phenotype we treated control induced astrocytes with pentostatin before adding motor neurons to the co-culture. We found that in the presence of adenosine (4 mM), ADA-inhibited control induced astrocytes become significantly more toxic towards motor neurons, mimicking the levels we observed in the ALS patients and reducing motor neuron survival by ~35% at 0.5 μM pentostatin (Fig. 7). This toxicity towards motor neurons became evident at pentostatin concentrations that were not toxic towards induced astrocytes (0.05–0.5 μM, Figs 3D and 7B).

Discussion

Our phenotypic metabolic screening approach in patient models of ALS has identified dysfunction in adenosine to inosine hydrolytic deamination (Fig. 1). This was confirmed by western blotting and RT-PCR showing lower levels of ADA, the enzyme responsible for deamination (Fig. 2). These findings have important implications for the role of effective nucleoside metabolism in ALS. A defect in the ability to metabolise adenosine could lead to accumulation of adenosine both intracellularly and extracellularly in the CNS culminating in enhanced neuronal toxicity. Higher adenosine levels have been observed in ALS patient CSF compared to controls (Yoshida *et al.*, 1999). Our data suggested that induced astrocytes from ALS patients were more susceptible to adenosine-mediated cell loss compared to controls, which could be mimicked by inhibiting ADA activity in control induced astrocytes (Fig. 3).

Under physiological conditions, both astrocytes and neurons release ATP, which functions as a key signalling molecule. ATP binds to purine receptors (P2XR and P2XY), impacting on astrocyte, oligodendrocyte, microglia and neuronal function, influencing the response to inflammation, calcium signalling and synaptic activity (Coco *et al.*, 2003; Larsson *et al.*, 2012). However, under stress or disease pathology conditions, when neurons can lose their structural integrity, ATP release increases significantly. This activates microglia and astrocytes causing increased astrogliosis and neuroinflammation, damage to oligodendrocytes and neuronal toxicity (Rothstein *et al.*, 1996). ATP levels can be reduced by the action of ectonucleotide-metabolizing enzymes, metabolising ATP to ADP, AMP and then adenosine (Volonte *et al.*, 2016). Physiological extracellular adenosine levels range between 25–250 nM, which may only be sufficient to activate high-affinity A1, A2a and A3 G-coupled receptors (A-Rs). However under stress or disease pathology conditions, ATP derived adenosine levels increase significantly and can activate low affinity receptors (A2b) (Dunwiddie and Masino, 2001). Outside the striatum, under physiological conditions, A2a-Rs are expressed at low levels by neurons, microglia and astrocytes. However, A2a-R expression increases following brain insults (Svenningsson *et al.*, 1999; Pickel *et al.*, 2006; Albasanz *et al.*, 2008; Yu *et al.*, 2008; Ng *et al.*, 2015). A2a-R expression increases astrocyte proliferation and activation, reduces glutamate uptake and stimulates calcium-dependent glutamate release. This loss of glutamate clearance leads to neuronal stress via glutamate-mediated excitotoxicity in ALS (Rothstein *et al.*, 1996). SNARE-dependent exocytosis of glutamate has been show to contribute to astrocyte-mediated motor neuron toxicity in the G93A SOD1 mouse model, which could be inhibited by the overexpression of dominant-negative SNARE (dnSNARE). This selective inhibition of exocytosis delayed disease onset in the SOD1 mice (Kawamata *et al.*, 2014). However, SNARE-mediated astrocyte glutamate stimulation of neurons is a hotly debated topic (Sloan and Barres, 2014). Data generated to study gliotransmission in transgenic dnSNARE mice were produced based on the premise that dnSNARE expression was limited to astrocytes. However, more recent data have uncovered cortical neuron expression of dnSNARE mice (Fujita *et al.*, 2014), which could have implications for how we believe astrocyte adenosine regulates neuronal processes.

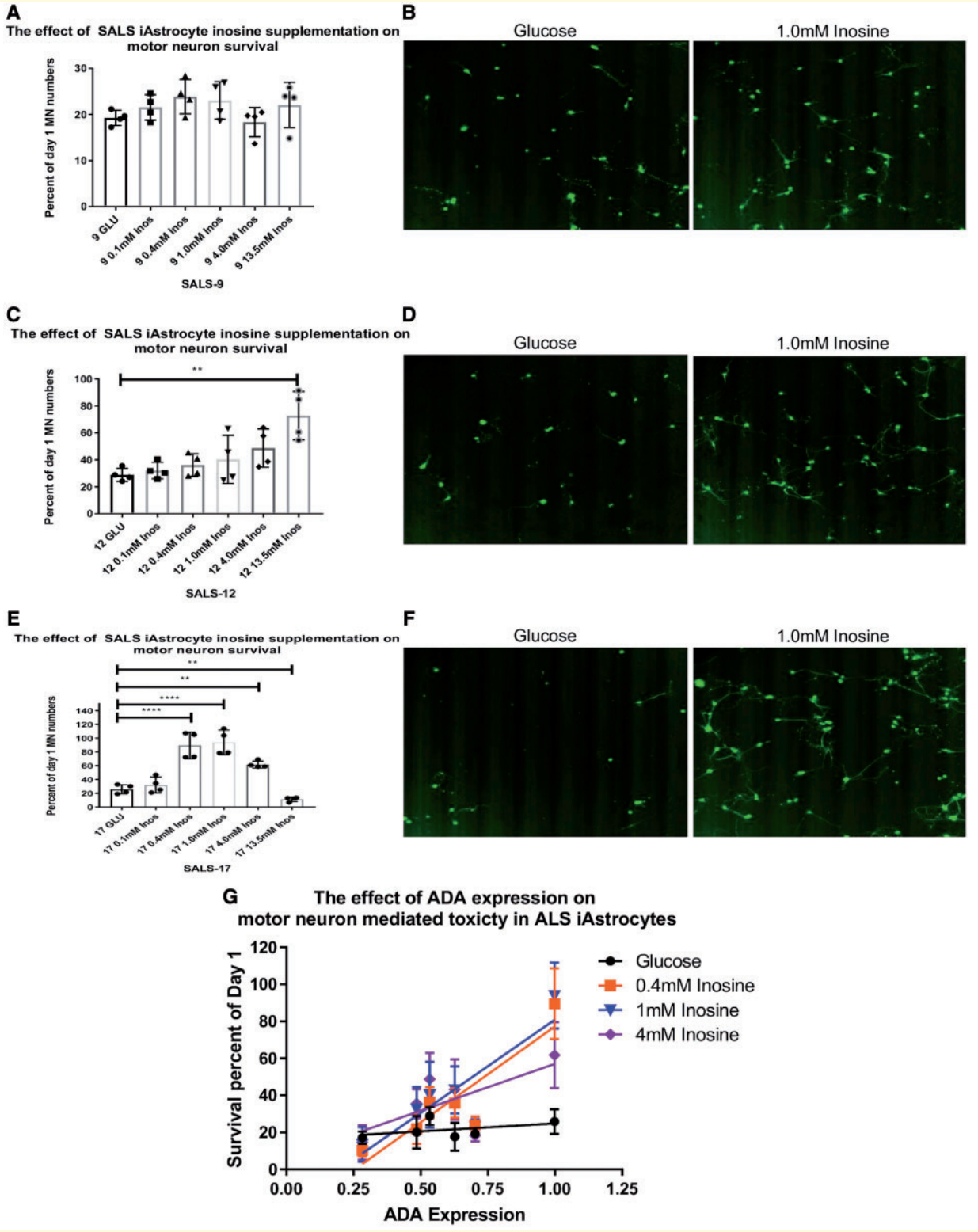

Figure 6 Sporadic ALS induced astrocyte inosine supplementation increases motor neuron survival in co-culture. Induced astrocytes were treated with 0.4–13.5 mM inosine for 24 h prior to 72-h co-culture with EGFP motor neurons (MN). (**A**) Number of motor neurons with axons after 72-h incubation with sporadic ALS-9 expressed as a percentage of the number alive at the start of the assay. (**C**) Number of motor neurons with axons after 72-h incubation with sporadic ALS-12 expressed as a percentage of the number alive at the start of the assay. (**E**) Number of motor neurons with axons after 72-h incubation with sporadic ALS-17 expressed as a percentage of the number alive at the start of the assay. (**B**, **D** and **F**) Representative images of the motor neurons after 72 h in glucose or glucose plus inosine. All data were transformed Y = 1/Y and Y = Logit(Y) prior to Kruskal Wallis analysis with a Dunn's post-test and are presented with mean and standard deviation. *$P \leqslant 0.05$, **$P \leqslant 0.01$, ***$P \leqslant 0.001$, ****$P \leqslant 0.0001$. (**G**) The effect of induced astrocyte ADA expression on motor neuron cell survival in the presence of glucose or inosine. Pearson's correlation analysis performed on the data, which is presented as the mean of cell survival with standard deviation. For Pearson's analysis results see Supplementary Table 3.

An increase in spinal cord A2a-R levels has been observed in the SOD1-G93A mice and in post-mortem ALS samples (Ng *et al.*, 2015). Contradictory studies have been published however, suggesting that both A2a-R antagonism and agonism are beneficial in mouse models of ALS, reducing motor neuron toxicity and delaying disease onset (Mojsilovic-Petrovic *et al.*, 2006; Impellizzeri *et al.*, 2011; Komaki *et al.*, 2012; Ng *et al.*, 2015). Blocking A2a-Rs would not primarily deal with the large pool of potentially toxic extracellular adenosine that may accumulate. Furthermore, due to bidirectional nucleoside transporters, this pool of adenosine could enter the cell and be reconverted back to ATP through the action of adenosine kinase (ADK). Historically, astrocytic ADK has been proposed to play the key role in the metabolic reuptake of adenosine in the adult brain (Pak *et al.*, 1994; Studer *et al.*, 2006; Ren *et al.*, 2007). However, in a model or state of neurodegeneration, intracellular ADK metabolism of adenosine, would propagate a cycle of increasing toxicity as more intracellular ATP would be formed, released and converted back into adenosine (Boison *et al.*, 2010). An alternative route of metabolism for adenosine is deamination to inosine by ADA. If ADA levels were reduced, too little adenosine would be removed from the cycle and this could lead to accumulation of toxic levels of adenosine over time.

In this present study, inhibiting ADA activity in control induced astrocytes by pentostatin led to decreased adenosine metabolism (Fig. 3F) and increased motor neuron death in co-culture (Fig. 7). This suggests that ADA levels and efficient adenosine to inosine deamination in the CNS may be important for astrocyte-motor neuron cross talk and that disruption of this process in astrocytes may increase motor neuron death. The fact that we have obtained a motor neuron death phenotype independently of a gene mutation has important implications not only for genetic models of ALS, but also sporadic ALS where we observe a similar loss of ADA.

ADA is a ubiquitous enzyme found both intracellularly and extracellularly, playing a role in purine homeostasis (Lindley and Pisoni, 1993). There are two isoforms of ADA and multiple mutations have been described that lead to disease (Whitmore and Gaspar, 2016). In cases of ADA loss, patients suffer from severe combined immunodeficiency due to a defect in T cell development. However, a clinical spectrum exists, including adult onset combined immunodeficiency and partial ADA deficiency. In general, enzyme activity in most identified ADA pathogenic missense and splice site variants correlate with a metabolic phenotype (Whitmore and Gaspar, 2016).

The role of ADA in ALS is unclear. In the SOD1 mouse model CD4+/CD25+/FoxP3 lymphocytes produce increased IL-4 early in the disease course, which in turn induces M2 protective microglia, indicating that T-cell deficiency could influence disease progression rates (Beers *et al.*, 2008; Chiu *et al.*, 2008; Liao *et al.*, 2012). Furthermore, oestradiol, which has been shown to activate *ADA* mRNA in breast cancer cells (Xie *et al.*, 2001) plays a protective role in ALS in pre-menopausal women (Klemann *et al.*, 2018) potentially via anti-inflammatory and neuronal protection mechanisms (Heitzer *et al.*, 2017). Our results suggest that loss of ADA activity in low levels of adenosine is not sufficient to cause toxicity. However, as soon as adenosine levels rise, the astrocytes become susceptible (Fig. 3). This may suggest that lower ADA levels in patients only become an issue in the presence of neuronal stress or disease pathology. ADA levels may however; affect disease progression rates in patients, as higher levels would potentially confer greater protection from adenosine-mediated toxicity in the CNS.

In this study, inosine was not toxic and in four of six patient lines (as well as all control lines) significantly reduced the induced astrocyte-mediated toxicity towards motor neurons. Inosine production via effective ADA expression has multiple cellular benefits. Production of uric acid from inosine via xanthine (Fang *et al.*, 2013) may confer neuroprotective effects including as an antioxidant (Chen *et al.*, 2012, 2013) with some studies pointing towards a positive relationship between serum uric acid concentrations and ALS disease progression/survival rates in males (Paganoni *et al.*, 2012; Oh *et al.*, 2015). We observed an increase in uric acid levels in induced astrocytes supplemented with inosine (Fig. 4K), including those from Patient 183, which showed no motor neuron survival increase. This indicates that the primary mechanism of reduced induced astrocyte-mediated toxicity towards motor neuron is not through increased uric acid production. Inosine can also be converted to ribose-1-phosphate by nucleoside phosphorylase, which feeds into the glycolytic pathway via the pentose phosphate pathway, producing NADH, ATP and subsequently lactate (Jurkowitz *et al.*, 1998; Balestri *et al.*, 2007). Lower induced astrocyte ADA levels may reduce the level of inosine in the cells leading to a decrease in the carbon flow into glycolysis, which may be crucial in the presence of an ATP deficit. Therefore, the decrease in induced astrocyte-mediated motor neuron toxicity we observed with inosine supplementation is likely due to the increased glycolytic capacity observed in induced astrocytes that perhaps leads to increased lactate production (Fig. 4H–J). Lactate deficiency has been linked to motor neuron toxicity in previous studies (Ferraiuolo *et al.*, 2011*a*, 2016).

Our metabolic screening approach has identified further points in the metabolic pathway in these patient-derived cells where dysfunction is evident (Fig. 1, Supplementary Figs 4 and 6) and these pathways will be investigated in detail in future work. It is evident from our data that the level of dysfunction is patient specific as would be expected in patient-derived cell lines with different genetic backgrounds, taken at different points during disease progression (Allen *et al.*, 2017). Our data suggest defects in pyruvate, glycogen, fructose and adenosine metabolism. Defects in pyruvate and glycogen metabolism have been

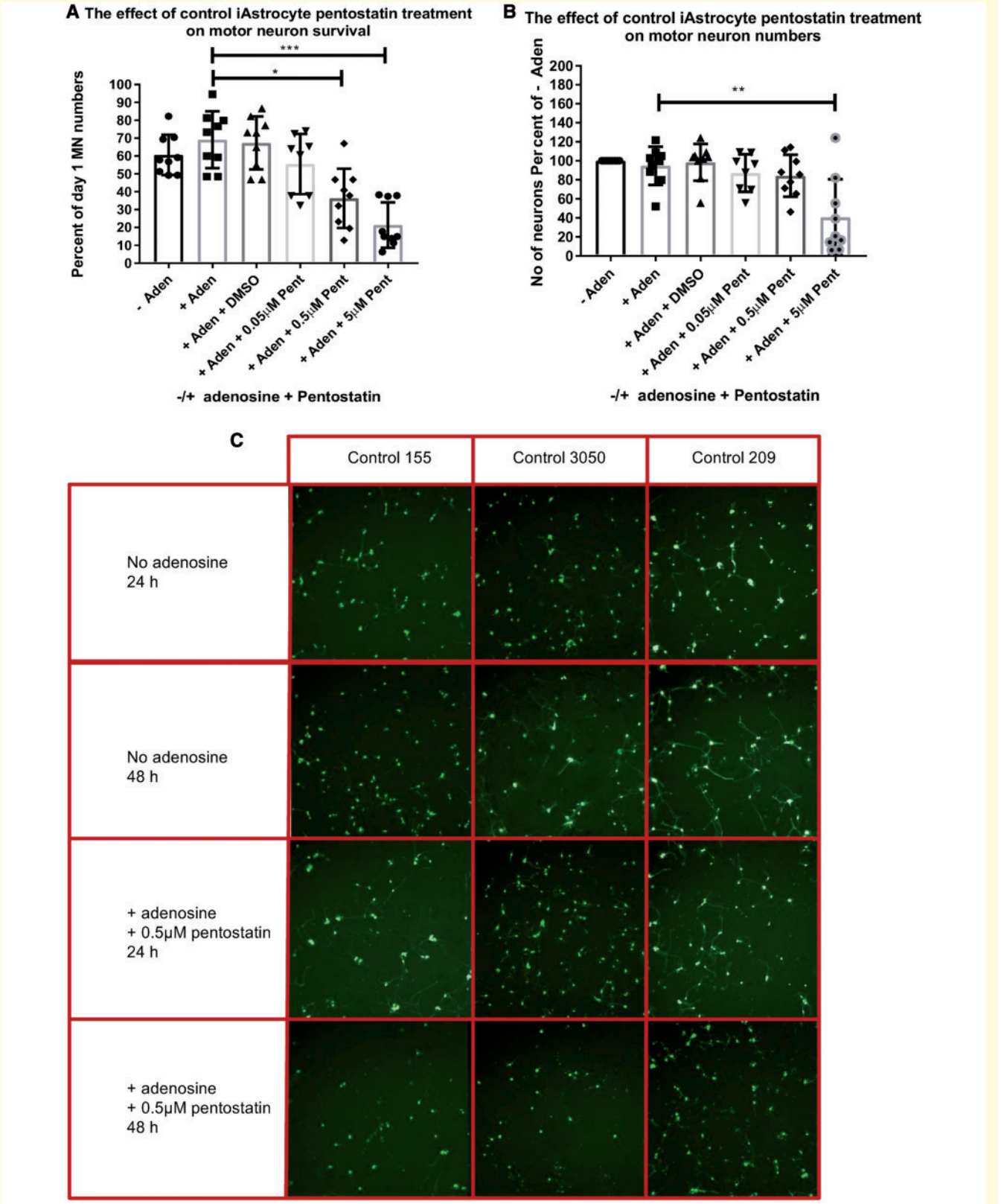

Figure 7 Inhibition of adenosine deaminase with pentostatin increases control induced astrocyte mediated toxicity towards motor neurons in the presence of adenosine. (**A**) Number of motor neurons (MN) with axons alive after 48 h, expressed as a percentage of the number alive at the start of the assay. (**B**) Number of motor neurons with axons at the start of the assay, expressed as a percentage of the glucose control. (**C**) Representative images of the three controls tested in triplicate. Control induced astrocytes were treated with pentostatin for 18 h prior to incubation with 4 mM adenosine for 24 h and then addition of EGFP motor neurons. All data were transformed Y = 1/Y and Y = Logit(Y) prior to Kruskal Wallis analysis with a Dunn's post-test and are presented with mean and standard deviation. *$P \leqslant 0.05$, **$P \leqslant 0.01$, ***$P \leqslant 0.001$.

observed previously in ALS models (Wiedemann *et al.*, 1998; Dodge *et al.*, 2013; Valbuena *et al.*, 2016; Tefera and Borges, 2018), inferring that common mechanisms of metabolic dysfunction potentially exist between *C9orf72*-HRE models of ALS and other genetic subtypes, as well as sporadic ALS models. Moreover, we can use the data generated to offer an explanation as to why one *C9orf72* patient and one sporadic ALS patient did not respond in the same way to inosine supplementation as in the other four patients. *C9orf72* Patient 183 showed the lowest level of NADH-production in the presence of pyruvic acid (Supplementary Fig. 4H), significantly lower than Patient 78. This was confirmed functionally, as no significant increase in glycolytic flux or lactate production was observed with this patient after inosine supplementation, which feeds into this pathway (Fig. 4G, H and J). Similar results were observed with Patient sALS-9, although it did not have the lowest NADH production in pyruvic acid (comparable to Patient sALS-17 but significantly lower than Patient sALS-12, Supplementary Fig. 6F), it had the lowest NADH production in the presence of lactic acid (Supplementary Fig. 6G). NADH production in Patient sALS-9 was significantly lower than Patient sALS-12 and 65% lower than Patient sALS-17 at the end-point of the assay. Furthermore, Patient sALS-9 showed no glycolytic ATP response to inosine supplementation (Supplementary Fig. 6J).

Our data have uncovered a common pathway of dysfunction that exists between *C9orf72* and sporadic ALS patients. The mechanism that triggers loss of ADA and the disease stage at which the defect occurs are unclear at this point. One possibility is that the level of ADA in patients may be protective and although no obvious correlation was observed between ADA levels and *C9orf72* expansion size or clinical characteristics, our data suggest a correlation between ADA level and extent of adenosine mediated toxicity in our six *C9orf72* and sporadic ALS patients (Fig. 7G). Furthermore, we observed a positive correlation between induced astrocyte ADA levels and extent of motor neuron survival in the presence of inosine (Fig. 6G). Purine feedback mechanisms have previously been reported in cancer cells with both inosine and hypoxanthine being reconverted to inosine monophosphate and eventually adenosine via AMP (Tolstikov *et al.*, 2014). A higher level of ADA could therefore feed into this system, producing more inosine, which could be shuttled into the ribose pathway. Work is underway in our laboratory to further investigate the role of ADA in ALS.

Acknowledgements

We thank all the ALS patients and control participants for donating biosamples to aid this research, supported by the NIHR Sheffield Biomedical Research Centre for Translational Neuroscience. Thanks to Dr Paul Heath for support on Qlucore, Dr Barry Bochner, Dr Serena Chan, Dr Eric Olender and Mr Andre Chouankam from Biolog and Mrs Frances Allen for technical support throughout this study.

Funding

We thank Neurocare, registered charity number 1169762-14 for funding the Seahorse XF24 bioanalyser and the OmniLog™ Phenotype system. This work was funded by a Motor Neurone Disease Association Senior Fellowship award to S.P.A. (grant number 956-799, MNDA-registered charity number 294354). M.R.T. is supported by the Medical Research Council and Motor Neurone Disease Association Lady Edith Wolfson Senior Clinical Fellowship (MR/K01014X/1). G.M.H. is supported by the Motor Neurone Disease Association grant Apr16/846-791. P.J.S. is supported by the Medical Research Council, the MND Association and as an NIHR Senior Investigator (grant number NF-SI-0617-10077). H.C.K. is supported by a FP7 project EuroMotor (Grant Agreement No. 259867), Cancer Research UK (Grant Agreement C19335/A21351) together with infrastructure support from the Imperial Experimental Cancer Medicine Centre & Cancer Research UK Centre. C.S.B. and K.J.D.V were funded by the UK Medical Research Council (MR/M013251/1 to K.J.D.V.). K.J.D.V and C.P.W. were funded by the Alzheimer's Society (260 (AS-PG-15-023)). The Sheffield NIHR Biomedical Research Centre provided support for this study.

Competing interests

The authors report no competing interests.

Supplementary material

Supplementary material is available at *Brain* online.

References

Al-Sarraj S, King A, Troakes C, Smith B, Maekawa S, Bodi I, et al. p62 positive, TDP-43 negative, neuronal cytoplasmic and intranuclear inclusions in the cerebellum and hippocampus define the pathology of C9orf72-linked FTLD and MND/ALS. Acta Neuropathol 2011; 122: 691–702.

Albasanz JL, Perez S, Barrachina M, Ferrer I, Martin M. Up-regulation of adenosine receptors in the frontal cortex in Alzheimer's disease. Brain Pathol 2008; 18: 211–9.

Allen CF, Shaw PJ, Ferraiuolo L. Can astrocytes be a target for precision medicine? Adv Exp Med Biol 2017; 1007: 111–28.

Allen SP, Duffy LM, Shaw PJ, Grierson AJ. Altered age-related changes in bioenergetic properties and mitochondrial morphology in fibroblasts from sporadic amyotrophic lateral sclerosis patients. Neurobiol Aging 2015; 36: 2893–903.

Allen SP, Rajan S, Duffy L, Mortiboys H, Higginbottom A, Grierson AJ, et al. Superoxide dismutase 1 mutation in a cellular model of amyotrophic lateral sclerosis shifts energy generation from oxidative

phosphorylation to glycolysis. Neurobiol Aging 2014; 35: 1499–509.
Balestri F, Giannecchini M, Sgarrella F, Carta MC, Tozzi MG, Camici M. Purine and pyrimidine nucleosides preserve human astrocytoma cell adenylate energy charge under ischemic conditions. Neurochem Int 2007; 50: 517–23.
Bartolome F, Wu HC, Burchell VS, Preza E, Wray S, Mahoney CJ, et al. Pathogenic VCP mutations induce mitochondrial uncoupling and reduced ATP levels. Neuron 2013; 78: 57–64.
Beers DR, Henkel JS, Zhao W, Wang J, Appel SH. CD4+ T cells support glial neuroprotection, slow disease progression, and modify glial morphology in an animal model of inherited ALS. Proc Natl Acad Sci USA 2008; 105: 15558–63.
Bochner BR, Siri M, Huang RH, Noble S, Lei XH, Clemons PA, et al. Assay of the multiple energy-producing pathways of mammalian cells. PloS One 2011; 6: e18147.
Boison D, Chen JF, Fredholm BB. Adenosine signaling and function in glial cells. Cell Death Differ 2010; 17: 1071–82.
Chen X, Burdett TC, Desjardins CA, Logan R, Cipriani S, Xu Y, et al. Disrupted and transgenic urate oxidase alter urate and dopaminergic neurodegeneration. Proc Natl Acad Sci USA 2013; 110: 300–5.
Chen X, Wu G, Schwarzschild MA. Urate in Parkinson's disease: more than a biomarker? Curr Neurol Neurosci Rep 2012; 12: 367–75.
Chiu IM, Chen A, Zheng Y, Kosaras B, Tsiftsoglou SA, Vartanian TK, et al. T lymphocytes potentiate endogenous neuroprotective inflammation in a mouse model of ALS. Proc Natl Acad Sci USA 2008; 105: 17913–8.
Coco S, Calegari F, Pravettoni E, Pozzi D, Taverna E, Rosa P, et al. Storage and release of ATP from astrocytes in culture. J Biol Chem 2003; 278: 1354–62.
Cooper-Knock J, Walsh MJ, Higginbottom A, Robin Highley J, Dickman MJ, Edbauer D, et al. Sequestration of multiple RNA recognition motif-containing proteins by C9orf72 repeat expansions. Brain 2014; 137: 2040–51.
De Vos KJ, Hafezparast M. Neurobiology of axonal transport defects in motor neuron diseases: opportunities for translational research? Neurobiol Dis 2017; 105: 283–99.
DeJesus-Hernandez M, Mackenzie IR, Boeve BF, Boxer AL, Baker M, Rutherford NJ, et al. Expanded GGGGCC hexanucleotide repeat in noncoding region of C9ORF72 causes chromosome 9p-linked FTD and ALS. Neuron 2011; 72: 245–56.
Desport JC, Preux PM, Truong TC, Vallat JM, Sautereau D, Couratier P. Nutritional status is a prognostic factor for survival in ALS patients. Neurology 1999; 53: 1059–63.
Desport JC, Torny F, Lacoste M, Preux PM, Couratier P. Hypermetabolism in ALS: correlations with clinical and paraclinical parameters. Neurodegener Dis 2005; 2: 202–7.
Dodge JC, Treleaven CM, Fidler JA, Tamsett TJ, Bao C, Searles M, et al. Metabolic signatures of amyotrophic lateral sclerosis reveal insights into disease pathogenesis. Proc Natl Acad Sci USA 2013; 110: 10812–7.
Dunwiddie TV, Masino SA. The role and regulation of adenosine in the central nervous system. Annu Rev Neurosci 2001; 24: 31–55.
Dupuis L, Pradat PF, Ludolph AC, Loeffler JP. Energy metabolism in amyotrophic lateral sclerosis. Lancet Neurol 2011; 10: 75–82.
Fang P, Li X, Luo JJ, Wang H, Yang XF. A double-edged sword: uric acid and neurological disorders. Brain Disord Ther 2013; 2: 109.
Ferraiuolo L, Higginbottom A, Heath PR, Barber S, Greenald D, Kirby J, et al. Dysregulation of astrocyte-motoneuron cross-talk in mutant superoxide dismutase 1-related amyotrophic lateral sclerosis. Brain 2011a; 134: 2627–41.
Ferraiuolo L, Kirby J, Grierson AJ, Sendtner M, Shaw PJ. Molecular pathways of motor neuron injury in amyotrophic lateral sclerosis. Nat Rev Neurol 2011b; 7: 616–30.
Ferraiuolo L, Meyer K, Sherwood TW, Vick J, Likhite S, Frakes A, et al. Oligodendrocytes contribute to motor neuron death in ALS via SOD1-dependent mechanism. Proc Natl Acad Sci USA 2016; 113: E6496–505.
Fujita T, Chen MJ, Li B, Smith NA, Peng W, Sun W, et al. Neuronal transgene expression in dominant-negative SNARE mice. J Neurosci 2014; 34: 16594–604.
Haeusler AR, Donnelly CJ, Rothstein JD. The expanding biology of the C9orf72 nucleotide repeat expansion in neurodegenerative disease. Nat Rev Neurosci 2016; 17: 383–95.
Haidet-Phillips AM, Hester ME, Miranda CJ, Meyer K, Braun L, Frakes A, et al. Astrocytes from familial and sporadic ALS patients are toxic to motor neurons. Nat Biotechnol 2011; 29: 824–8.
Hautbergue GM, Castelli LM, Ferraiuolo L, Sanchez-Martinez A, Cooper-Knock J, Higginbottom A, et al. SRSF1-dependent nuclear export inhibition of C9ORF72 repeat transcripts prevents neurodegeneration and associated motor deficits. Nat Commun 2017; 8: 16063.
Heitzer M, Kaiser S, Kanagaratnam M, Zendedel A, Hartmann P, Beyer C, et al. Administration of 17beta-estradiol improves motoneuron survival and down-regulates inflammasome activation in male SOD1(G93A) ALS mice. Mol Neurobiol 2017; 54: 8429–43.
Impellizzeri D, Di Paola R, Esposito E, Mazzon E, Paterniti I, Melani A, et al. CGS 21680, an agonist of the adenosine (A2A) receptor, decreases acute lung inflammation. Eur J Pharmacol 2011; 668: 305–16.
Jurkowitz MS, Litsky ML, Browning MJ, Hohl CM. Adenosine, inosine, and guanosine protect glial cells during glucose deprivation and mitochondrial inhibition: correlation between protection and ATP preservation. J Neurochem 1998; 71: 535–48.
Kawamata H, Ng SK, Diaz N, Burstein S, Morel L, Osgood A, et al. Abnormal intracellular calcium signaling and SNARE-dependent exocytosis contributes to SOD1G93A astrocyte-mediated toxicity in amyotrophic lateral sclerosis. J Neurosci 2014; 34: 2331–48.
Klemann CJ, Visser JE, Van Den Bosch L, Martens GJ, Poelmans G. Integrated molecular landscape of amyotrophic lateral sclerosis provides insights into disease etiology. Brain Pathol 2018; 28: 203–11.
Komaki S, Ishikawa K, Arakawa Y. Trk and cAMP-dependent survival activity of adenosine A(2A) agonist CGS21680 on rat motoneurons in culture. Neurosci Lett 2012; 522: 21–4.
Konrad C, Kawamata H, Bredvik KG, Arreguin AJ, Cajamarca SA, Hupf JC, et al. Fibroblast bioenergetics to classify amyotrophic lateral sclerosis patients. Mol Neurodegener 2017; 12: 76.
Larsson M, Sawada K, Morland C, Hiasa M, Ormel L, Moriyama Y, et al. Functional and anatomical identification of a vesicular transporter mediating neuronal ATP release. Cereb Cortex 2012; 22: 1203–14.
Liao B, Zhao W, Beers DR, Henkel JS, Appel SH. Transformation from a neuroprotective to a neurotoxic microglial phenotype in a mouse model of ALS. Exp Neurol 2012; 237: 147–52.
Lin CL, Bristol LA, Jin L, Dykes-Hoberg M, Crawford T, Clawson L, et al. Aberrant RNA processing in a neurodegenerative disease: the cause for absent EAAT2, a glutamate transporter, in amyotrophic lateral sclerosis. Neuron 1998; 20: 589–602.
Lindley ER, Pisoni RL. Demonstration of adenosine deaminase activity in human fibroblast lysosomes. Biochem J 1993; 290 (Pt 2): 457–62.
Lopez-Gonzalez R, Lu Y, Gendron TF, Karydas A, Tran H, Yang D, et al. Poly(GR) in C9ORF72-related ALS/FTD compromises mitochondrial function and increases oxidative stress and DNA damage in iPSC-derived motor neurons. Neuron 2016; 92: 383–91.
Meyer K, Ferraiuolo L, Miranda CJ, Likhite S, McElroy S, Renusch S, et al. Direct conversion of patient fibroblasts demonstrates non-cell autonomous toxicity of astrocytes to motor neurons in familial and sporadic ALS. Proc Natl Acad Sci USA 2014; 111: 829–32.
Mojsilovic-Petrovic J, Jeong GB, Crocker A, Arneja A, David S, Russell DS, et al. Protecting motor neurons from toxic insult by antagonism of adenosine A2a and Trk receptors. J Neurosci 2006; 26: 9250–63.
Mori K, Arzberger T, Grasser FA, Gijselinck I, May S, Rentzsch K, et al. Bidirectional transcripts of the expanded C9orf72

hexanucleotide repeat are translated into aggregating dipeptide repeat proteins. Acta Neuropathol 2013a; 126: 881–93.
Mori K, Lammich S, Mackenzie IR, Forne I, Zilow S, Kretzschmar H, et al. hnRNP A3 binds to GGGGCC repeats and is a constituent of p62-positive/TDP43-negative inclusions in the hippocampus of patients with C9orf72 mutations. Acta Neuropathol 2013b; 125: 413–23.
Mori K, Weng SM, Arzberger T, May S, Rentzsch K, Kremmer E, et al. The C9orf72 GGGGCC repeat is translated into aggregating dipeptide-repeat proteins in FTLD/ALS. Science 2013c; 339: 1335–8.
Ng SK, Higashimori H, Tolman M, Yang Y. Suppression of adenosine 2a receptor (A2aR)-mediated adenosine signaling improves disease phenotypes in a mouse model of amyotrophic lateral sclerosis. Exp Neurol 2015; 267: 115–22.
Oh SI, Baek S, Park JS, Piao L, Oh KW, Kim SH. Prognostic role of serum levels of uric acid in amyotrophic lateral sclerosis. J Clin Neurol 2015; 11: 376–82.
Onesto E, Colombrita C, Gumina V, Borghi MO, Dusi S, Doretti A, et al. Gene-specific mitochondria dysfunctions in human TARDBP and C9ORF72 fibroblasts. Acta Neuropathol Commun 2016; 4: 47.
Paganoni S, Zhang M, Quiroz Zarate A, Jaffa M, Yu H, Cudkowicz ME, et al. Uric acid levels predict survival in men with amyotrophic lateral sclerosis. J Neurol 2012; 259: 1923–8.
Pak MA, Haas HL, Decking UK, Schrader J. Inhibition of adenosine kinase increases endogenous adenosine and depresses neuronal activity in hippocampal slices. Neuropharmacology 1994; 33: 1049–53.
Pellerin L, Magistretti PJ. Glutamate uptake into astrocytes stimulates aerobic glycolysis: a mechanism coupling neuronal activity to glucose utilization. Proc Natl Acad Sci USA 1994; 91: 10625–9.
Pickel VM, Chan J, Linden J, Rosin DL. Subcellular distributions of adenosine A1 and A2A receptors in the rat dorsomedial nucleus of the solitary tract at the level of the area postrema. Synapse 2006; 60: 496–509.
Raman R, Allen SP, Goodall EF, Kramer S, Ponger LL, Heath PR, et al. Gene expression signatures in motor neurone disease fibroblasts reveal dysregulation of metabolism, hypoxia-response and RNA processing functions. Neuropathol Appl Neurobiol 2015; 41: 201–26.
Re DB, Le Verche V, Yu C, Amoroso MW, Politi KA, Phani S, et al. Necroptosis drives motor neuron death in models of both sporadic and familial ALS. Neuron 2014; 81: 1001–8.
Ren G, Li T, Lan JQ, Wilz A, Simon RP, Boison D. Lentiviral RNAi-induced downregulation of adenosine kinase in human mesenchymal stem cell grafts: a novel perspective for seizure control. Exp Neurol 2007; 208: 26–37.
Rothstein JD, Dykes-Hoberg M, Pardo CA, Bristol LA, Jin L, Kuncl RW, et al. Knockout of glutamate transporters reveals a major role for astroglial transport in excitotoxicity and clearance of glutamate. Neuron 1996; 16: 675–86.
Saura J, Tusell JM, Serratosa J. High-yield isolation of murine microglia by mild trypsinization. Glia 2003; 44: 183–9.
Sloan SA, Barres BA. Looks can be deceiving: reconsidering the evidence for gliotransmission. Neuron 2014; 84: 1112–5.
Studer FE, Fedele DE, Marowsky A, Schwerdel C, Wernli K, Vogt K, et al. Shift of adenosine kinase expression from neurons to astrocytes during postnatal development suggests dual functionality of the enzyme. Neuroscience 2006; 142: 125–37.
Svenningsson P, Le Moine C, Fisone G, Fredholm BB. Distribution, biochemistry and function of striatal adenosine A2A receptors. Prog Neurobiol 1999; 59: 355–96.
Tefera TW, Borges K. Metabolic dysfunctions in amyotrophic lateral sclerosis pathogenesis and potential metabolic treatments. Front Neurosci 2016; 10: 611.
Tefera TW, Borges K. Neuronal glucose metabolism is impaired while astrocytic TCA cycling is unaffected at symptomatic stages in the hSOD1(G93A) mouse model of amyotrophic lateral sclerosis. J Cereb Blood Flow Metab 2018: 271678X18764775. doi: 10.1177/0271678X18764775.
Tolstikov V, Nikolayev A, Dong S, Zhao G, Kuo MS. Metabolomics analysis of metabolic effects of nicotinamide phosphoribosyltransferase (NAMPT) inhibition on human cancer cells. PloS One 2014; 9: e114019.
Valbuena GN, Rizzardini M, Cimini S, Siskos AP, Bendotti C, Cantoni L, et al. Metabolomic analysis reveals increased aerobic glycolysis and amino acid deficit in a cellular model of amyotrophic lateral sclerosis. Mol Neurobiol 2016; 53: 2222–40.
Vandoorne T, De Bock K, Van Den Bosch L. Energy metabolism in ALS: an underappreciated opportunity? Acta Neuropathol 2018; 135: 489–509.
Volonte C, Apolloni S, Parisi C, Amadio S. Purinergic contribution to amyotrophic lateral sclerosis. Neuropharmacology 2016; 104: 180–93.
Webster CP, Smith EF, Bauer CS, Moller A, Hautbergue GM, Ferraiuolo L, et al. The C9orf72 protein interacts with Rab1a and the ULK1 complex to regulate initiation of autophagy. EMBO J 2016; 35: 1656–76.
Whitmore KV, Gaspar HB. Adenosine deaminase deficiency—more than just an immunodeficiency. Front Immunol 2016; 7: 314.
Wiedemann FR, Winkler K, Kuznetsov AV, Bartels C, Vielhaber S, Feistner H, et al. Impairment of mitochondrial function in skeletal muscle of patients with amyotrophic lateral sclerosis. J Neurol Sci 1998; 156: 65–72.
Xie W, Duan R, Safe S. Activation of adenosine deaminase in MCF-7 cells through IGF-estrogen receptor alpha crosstalk. J Mol Endocrinol 2001; 26: 217–28.
Yoshida Y, Une F, Utatsu Y, Nomoto M, Furukawa Y, Maruyama Y, et al. Adenosine and neopterin levels in cerebrospinal fluid of patients with neurological disorders. Intern Med 1999; 38: 133–9.
Yu L, Shen HY, Coelho JE, Araujo IM, Huang QY, Day YJ, et al. Adenosine A2A receptor antagonists exert motor and neuroprotective effects by distinct cellular mechanisms. Ann Neurol 2008; 63: 338–46.